UCRL- 93136
PREPRINT

EXPERIMENTAL TEST OF MCDOUGALL'S THEORY FOR THE ONSET OF CONVECTIVE STABILITIES IN ISOTHERMAL TERNARY SYSTEMS

Donald G. Miller
and
Vincenzo Vitagliano

This paper was prepared for submittal to
J. Physical Chemistry

July 25, 1985

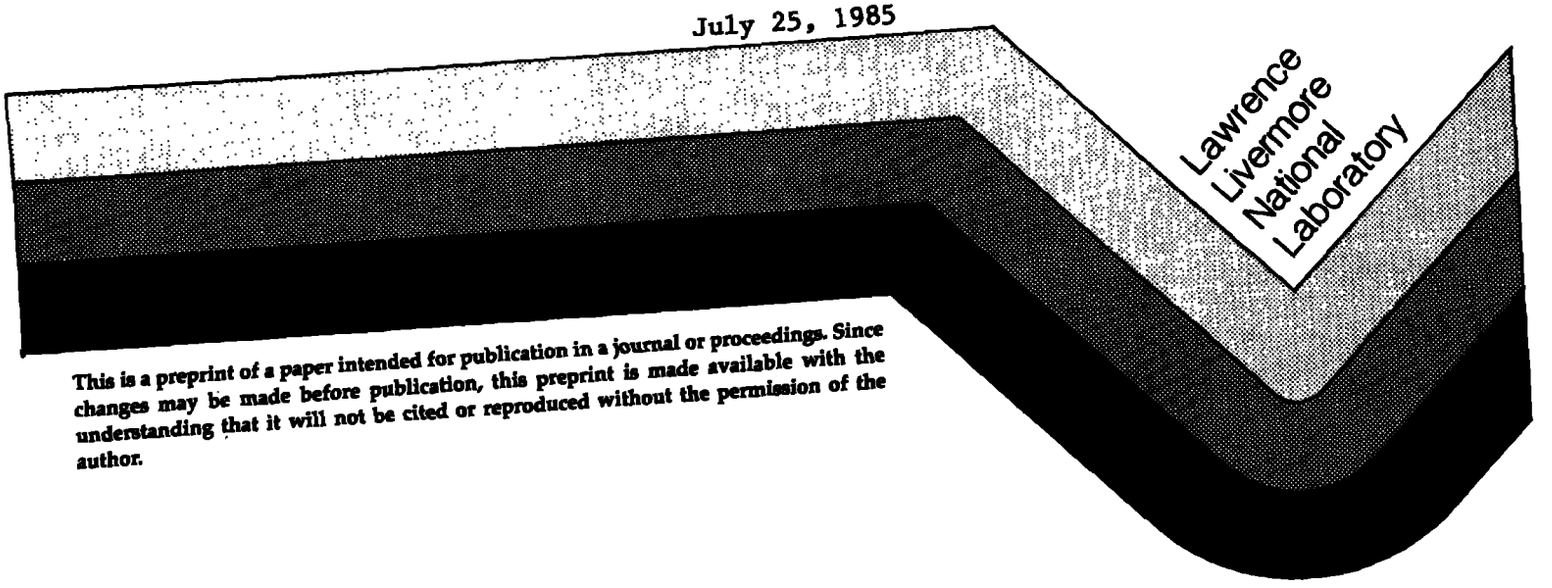

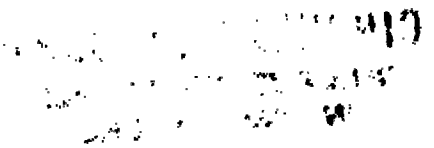

EXPERIMENTAL TEST OF MCDOUGALL'S THEORY FOR THE ONSET OF CONVECTIVE INSTABILITIES IN ISOTHERMAL TERNARY SYSTEMS

Donald G. Miller* and Vincenzo Vitagliano
Chemistry and Materials Sciences Department
Lawrence Livermore National Laboratory
P. O. Box 808
Livermore, CA 94550

ABSTRACT

The dynamic theory of McDougall for convective instabilities induced by isothermal diffusion has been tested experimentally. These experiments, using two homogeneous layers separated initially by a sharp boundary (free diffusion), were done on the ternary system $SrCl_2$(0.5M)-NaCl(0.5M)-H_2O, chosen because of its large cross-term diffusion coefficients. The experiments accurately verify McDougall's theory for the onset of the fingering instability at the center of the boundary. As predicted, this instability occurs first for compositions where the system is statically stable, i.e., no diffusion-induced density inversion. At boundary edges, density inversion and dynamic instability of the diffusive-overstable type begin simultaneously. The experiments are consistent with theory, although instabilities were not detected as close to the onset point as for fingering. Optical arrangements are described which are sensitive enough to detect the instabilities. Theoretical consequences of the free diffusion boundary conditions are that 1) at the edges the fingering instability condition is proportional to the static-diffusive one, and 2) the onset compositions at the edges depend only on D_{ij}, whereas fingering at the center depends on H_i as well.

1. INTRODUCTION

In recent years, the occurrence of convective instabilities has been observed or postulated in a wide variety of phenomena which involve diffusion.[1,2] These instabilities involve at least two diffusive components, which may include heat, matter, magnetic field, angular momentum, etc. When there are just two, the process is called double diffusive convection (DDC).

Examples of DDC are the heat-salt diffusivities which give rise to fingering in the oceans[1,2] and the isothermal diffusivities of two solutes which can give rise to convections which ruin measurements of diffusion coefficients.[3,4,5] Depending on experimental circumstances, convection can destroy boundaries either at the center or at both edges. Generally "fingering" is observed at the center, and "diffusive" or "overstable" interfaces at the edges. The term overstable was used in a more restricted sense by Vitagliano et al[3] because frequently the boundary edges appear to remain in position for long times, rather than spreading as expected.

Other examples[1,2] include applications in lakes and solar ponds, rollover in Liquid Natural Gas tanks, oceanography (steps arising from an initially smooth stratification), geology (crystallization and magma chamber processes), geophysics (mantle convection and vulcanism), metallurgy (morphology and crystallization), and polymer solutions. In these examples the driving force for convection is the gravitational potential, even though it is small with respect to the free energy change.

The above phenomena are usually called <u>dynamic</u> instabilities. There are also <u>static (gravitational)</u> instabilities. These can occur in a system whose top solution is initially less dense than the bottom one, i.e., initially statically stable. If the experimental conditions and diffusion coefficients have appropriate values, the diffusion process can cause a density reversal, and thus a convective

instability. Depending on the conditions, such static instabilities may occur either in the center or at the edges of the boundary. An obvious limiting case is "solution overturn" where the top solution is initially heavier than the bottom one. These static instabilities were investigated by Wendt[6] for 2 and 3 component systems, and by Kim[7] for 4 and more components.

At a 1983 conference,[8] there was considerable discussion about whether density reversals were necessary for dynamic instabilities or whether dynamic instabilities could arise in systems predicted to be statically stable. Some interesting results of Huppert and Manins[9] on isothermal diffusing systems had indicated dynamic instabilities (fingering) in statically stable systems. However, the experiments used large concentration differences in systems whose diffusion coefficients were not known, and depended on a theory which assumed cross-terms were zero. Other experiments by Preston, Comper and co-workers[10,11] on polymer mixtures indicated density reversals were required, but again the density and diffusion data are not well known. Clearly to resolve this question, careful experiments on well-characterized systems must be compared with a theory which includes cross-terms.

The theory of DDC is usually cast in terms of the heat-salt situation of oceanography.[1,2] However, with temperature gradients, a precise laboratory test is extremely difficult because it is nearly impossible to maintain the confining walls at the changing temperature distribution of the solution. Moreover, in the heat-salt case, the diffusivity of heat is about 100 times that of salt, and the heat-salt interaction coefficient (Soret coefficient) is small. Therefore, little choice is available in adjusting experimental conditions to magnify the precision of the test or to see the effects of cross-terms. Moreover, values of the thermal diffusivity, salt diffusivity, and Soret coefficients are poorly known or unavailable over the full-range of experimental conditions.

Experimental problems are somewhat less for isothermal ternary systems with two diffusing solutes: Isothermal conditions are easy to maintain, and the diffusivities can be chosen to be much closer with an appropriate choice of components, e.g., factors of 1-4. Moreover, the experiments can be done at a composition where the density and diffusion properties are known. Finally, it is easy to set up free diffusion (a sharp initial boundary) between two homogeneous solutions whose compositions are not very different; in this circumstance any concentration dependence of the diffusion coefficients may safely be neglected.

McDougall[12,13] has recently provided a linear dynamical theory for ternary isothermal systems, which includes non-zero cross-term diffusion coefficients for both the fingering and diffusive (overstable) cases. His results indicate that large cross-terms could have a substantial effect on the conditions for the onset of instabilities.

McDougall's results,[13] together with those of Wendt[6] and Kim,[7] permit a direct comparison of the predictions of both static and dynamic theories for the edges and center of an initially sharp boundary. Required are systems with known densities and diffusion coefficients, and a detection system sensitive enough to indicate where boundary disturbances occur.

An important first step was taken by Huppert and Hallworth,[14] who sought out systems with very small cross-terms over a wide composition range. Again, the fingering instability was found to occur in three systems predicted to be statically stable. The shadowgraph technique was used to observe the instabilities, but unfortunately quite large concentration differences are required. As they note, the dynamic instability criteria remain to be tested when cross-terms are large, both for the onset of disturbances at the center and at the edges.

Support for Huppert and Hallworth's conclusions was also provided by Vitagliano.[15] They analyzed existing schlieren data for the system $NaCl-NH_4Cl-H_2O$,[5] which has a non-negligible cross-term D_{21}. The data are quite consistent with McDougall's theory,[13] both for fingering at the center of a boundary predicted to be density stable and for overstability at the edges. Unfortunately, the compositions are not sufficiently close to the conditions for the onset of these phenomena to test the theoretical instability criteria in detail.

For free diffusion boundary conditions (sharp initial boundary) in liquids, it can be shown (1) that the diffusive (overstable) criteria are identical to the static (gravitational) criteria everywhere throughout the boundary,[15,16] and (2) that at the edges of the boundary, the fingering criterion is proportional to the static-diffusive criterion.[17] These results partially explain the results of Preston et al.[10,11] On the other hand, the fingering instability can occur even when the system is statically or diffusively stable, which explains the results of Huppert et al[9,14] and Kim.[18]

In this paper, we examine experimentally the predictions for the onset of instabilities from free diffusion boundaries for both static and dynamic stability theories, including the fingering and diffusive (overstable) cases. We have used the system $SrCl_2$(0.5M)-NaCl(0.5M)-H_2O, whose cross-terms are substantial.[19] Here M denotes the molarity. Relatively small concentration differences have been used to minimize concentration dependence. Four optical arrangements are sensitive enough to be used with small concentration differences. These are Rayleigh, modified Gouy, Schlieren, and "single slit Rayleigh". Singly or in conjunction, the last three arrangements allowed us to determine where the abnormalities are in the boundary.

For our system with large cross-terms, we find that the dynamic theory criterion for the onset of fingering at the boundary center is closely confirmed

within the sensitivity of our measurements. The onset of instability at the edges is consistent with the static/overstable/fingering criterion, but the instabilities are only detected somewhat inside the predicted onset point. A posible explanation is that the diffusion driving force dc_i/dx is less at the edges than at the center for a given Δc_i.

In a companion paper, Vitagliano et al.[20] have obtained similar results for the system sucrose(0.1M)-NaCl(0.3M)-H_2O, using schlieren and Rayleigh optics to examine boundary disturbances. This system has small cross-term D_{ij} when H_2O is assumed to be the solvent. However, they point out that the choice of solvent is arbitrary, and when sucrose or NaCl is chosen as solvent, the transformations[21,22] can give rise to large cross-terms. Thus, concentrating on systems with small cross-terms is also arbitrary.

We will conclude that in terms of the 1983 controversy, the partisans of the dynamic theory are correct for the case of fingering at the center of the boundary, and that both sides are correct for static/diffusive/fingering at the edges of the boundary.

2. CONDITIONS FOR INSTABILITY AT A FREE DIFFUSION BOUNDARY

McDougall's theory for both kinds of dynamic stability can be rewritten[15,16,17] in the notation customarily used by experimentalists doing liquid diffusion measurements.[23,24] In particular, mole units are used; constituent 2 is the faster moving solute; and the vertical distance x is positive going downwards. All inequalities indicate conditions for <u>instability</u>.

Depending on the application, inequalities can be written either as conditions independent of the signs of Δc_i, D_{ij}, and H_i,[17] or as conditions on $\Delta c_2/\Delta c_1$.[15]

The latter may require an analysis of the signs of Δc_i, D_{ij} and H_i. Here c_i are the concentrations of solutes 1 and 2 in moles-dm^{-3}, D_{ij} are the diffusion coefficients in cm-s^{-1} on the volume-fixed reference frame, and H_i are the coefficients $\partial\rho/\partial c_i$ in the linear density equation.

$$\rho(c_1,c_2) = \rho(\bar{c}_1,\bar{c}_2) + H_1(c_1-\bar{c}_1) + H_2(c_2-\bar{c}_2) \tag{1}$$

($H_1 = \beta, H_2 = \alpha$ in Ref. 15, $\bar{c_i}$ is the average concentration of solute i, ρ is the density in g-cm^{-3}, and Δ of a property P is [P(bottom) - P(top)].

2.1 General Conditions

We summarize the various <u>instability</u> conditions.

First, a system whose top solution is more dense than its bottom is unstable. This can be written[13,17] in terms of a stability function S

$$S_m = \Delta\rho = H_1\Delta c_1 + H_2\Delta c_2 < 0 \tag{2}$$

independent of the signs of H_i and Δc_i, or as Ref. 15.

$$S_v = \frac{\Delta c_2}{\Delta c_1} \begin{matrix} < \\ > \end{matrix} \frac{-H_1}{H_2} \tag{3}$$

where the direction of the inequality sign depends on the signs of Δc_i and H_i. Eq. 2 and 3 are the conditions for <u>solution overturn</u>; an equality sign will give the <u>neutral density</u> line.

For static (gravitational) instability, the result of Wendt[6] in one dimension can be written in terms of a function G'

$$G_m' = \frac{d\rho}{dx} = H_1\frac{\partial c_1}{\partial x} + H_2\frac{\partial c_2}{\partial x} < 0 \tag{4}$$

where $\partial c_1/\partial x$ are obtained from the solutions for appropriate boundary conditions of the diffusion equations

$$\frac{\partial c_1}{\partial t} = D_{11} \frac{\partial^2 c_1}{\partial x^2} + D_{12} \frac{\partial^2 c_2}{\partial x^2} \tag{5}$$

$$\frac{\partial c_2}{\partial t} = D_{21} \frac{\partial^2 c_1}{\partial x^2} + D_{22} \frac{\partial^2 c_2}{\partial x^2} \tag{6}$$

and t is the time in s. Alternatively, depending on the signs of dc_i and H_i

$$G_v' = \frac{\partial c_2}{\partial c_1} \begin{matrix} > \\ < \end{matrix} - \frac{H_1}{H_2} \tag{7}$$

McDougall's conditions for dynamic instability of the diffusive (overstable) type have been shown by Vitagliano et al.[15] and Tyrrell[16] to reduce to the static conditions G' of Equation 4 or 7 for liquids. This happens because D_{ij} are small compared to ρ and viscosity η; their result is valid everywhere in an arbitrary boundary.

For the fingering instability in an arbitrary boundary, the McDougall conditions can be written independently of the signs of dc_i, D_{ij}, and H_i as[17]

$$F_m' = F_A \frac{\partial c_1}{\partial x} + F_B \frac{\partial c_2}{\partial x} < 0 \tag{8}$$

where

$$F_A = H_1 D_{22} - H_2 D_{21} \tag{9}$$

$$F_B = H_2 D_{11} - H_1 D_{12} \tag{10}$$

or alternatively depending on the signs of dc_i, D_{ij}, and H_i

$$F_v' = \frac{\partial c_2}{\partial c_1} \begin{matrix} < \\ > \end{matrix} - \frac{F_A}{F_B} \tag{11}$$

Care with signs must be taken because there are systems with H_i and even negative D_{11}.[21,22]

2.2 Free Diffusion Conditions

We now specialize to the free diffusion case.[13,15,17] It is the easiest to set up for precision optical measurements,[24] being the diffusion of two long columns of solution into each other across an initially sharp interface. The solutions of Equations (5), (6) for this case[23] are

$$\frac{\partial c_i}{\partial x} = \frac{1}{2(\pi t)^{1/2}} \left[K_{ip} \frac{d\ \mathrm{erf}(s_1 y)}{dy} + K_{im} \frac{d\ \mathrm{erf}(s_2 y)}{dy}\right]$$

$$= \frac{s_2}{2(\pi t^{1/2})} \cdot \exp(-s_2^2 y^2)[K_{ip} w + K_{im}] \tag{12}$$

where

$$s_i = \sigma_i^{1/2} \tag{13}$$

$$\sigma_1 = \frac{D_{22} + D_{11} + Z}{2D} \tag{14}$$

$$\sigma_2 = \frac{D_{22} + D_{11} - Z}{2D} \tag{15}$$

$$Z = [(D_{11} + D_{22})^2 - 4D]^{1/2} = [A^2 + 4D_{12}D_{21}]^{1/2} \tag{16}$$

$$A = D_{22} - D_{11} \tag{17}$$

$$D = D_{11}D_{22} - D_{12}D_{21} \tag{18}$$

$$K_{1p} = \frac{p_1\Delta c_1 - q_1\Delta c_2}{4Z} \tag{19}$$

$$K_{1m} = \frac{p_2\Delta c_1 + q_1\Delta c_2}{4Z} \tag{20}$$

$$p_1 = A + Z \tag{21}$$

$$p_2 = -A + Z \tag{22}$$

$$q_1 = 2D_{12} \tag{23}$$

$$q_2 = 2D_{21} \tag{24}$$

and K_{2p} and K_{2m} are obtained by interchanging 1 and 2 in K_{1p} and K_{1m} respectively. Finally, w and y are given by

$$w = \frac{s_1}{s_2} \exp\left[-y^2(s_1^2 - s_2^2)\right] \tag{25}$$

$$y = \frac{x}{2t^{1/2}} \tag{26}$$

The quantities s_1, s_2, s_1-s_2, and w are all positive when $D_{11} < D_{22}$, hence w runs from s_1/s_2 at y = 0 (center of boundary) to 0 at y = ∞ (edges of boundary). The σ_i are the reciprocals of the eigenvalues of the diffusion matrix.[22]

Eq. 12 can be substituted into the instability criteria Eq. 4, 7, 8, 11. After cancellation or factoring out known positive quantities, the following results are obtained.

For the static-overstable case, we obtain for G_m [17]

$$G_m = G_1\Delta c_1 + G_2\Delta c_2 \tag{27}$$

where

$$G_1 = H_1(wp_1 + p_2) + H_2q_2(1-w) \tag{28}$$

$$G_2 = H_1q_1(1-w) + H_2(p_1 + wp_2) \tag{29}$$

The expression for G_v can be obtained from Eq. 33 of Vitagliano[15] plus the assumption that η is large:

$$G_v = \frac{\Delta c_2}{\Delta c_1} \begin{matrix} < \\ > \end{matrix} \frac{(A-BZ) - 2D_{21}(H_2/H_1)}{(A+BZ)(H_2/H_1) + 2D_{12}} \tag{30}$$

where the direction of the inequality sign depends on the signs of Δc_i, D_{ij}, and H_i, and where

$$B = \frac{1+w}{1-w} \tag{31}$$

For the fingering case, we obtain[17] independent of signs

$$F_m = F_1\Delta c_1 + F_2\Delta c_2 < 0 \tag{32}$$

$$F_1 = F_A(wp_1 + p_2) + F_Bq_2(1-w) \tag{33}$$

$$F_2 = F_Aq_1(1-w) + F_B(p_1+wp_2) \tag{34}$$

and from Eq. 32 of Vitagliano et al.[15] with misprints corrected, we get

$$F_v = \frac{\Delta c_2}{\Delta c_1} \begin{matrix} < \\ > \end{matrix} \frac{(\frac{H_2}{H_1}\frac{D_{21}}{D_{11}} - \frac{D_{22}}{D_{11}})(A-BZ) - 2D_{21}(\frac{D_{12}}{D_{11}} - \frac{H_2}{H_1})}{(\frac{D_{12}}{D_{11}} - \frac{H_2}{H_1})(A+BZ) + 2D_{12}(\frac{D_{21}}{D_{11}}\frac{H_2}{H_1} - \frac{D_{22}}{D_{11}})} \tag{35}$$

which depends on signs of Δc_i, D_{ij}, and H_i.

In all the conditions, an <u>equality</u> sign yields the point of the <u>onset</u> of instability.

For free diffusion, $\partial c_i/\partial x$ are symmetric about the center of the boundary. Therefore between the center and the edges, the $\partial c_i/\partial x$ change monotonically. By eq. 4 and 8, the static and dynamic instability conditions also change monotonically, with their extrema at the center and at the edges. Consequently, the onset of each type of instability will begin first either at the center or at the edges. We denote the center (y=0) and the edges ($y\to\infty$) by superscripts o and ∞ respectively.

It can be shown[17] that the fingering criterion at the edges is proportional to the static-gravitational one; namely,

$$G_m^\infty = \sigma_1 F_m^\infty \tag{36}$$

$$G_v^\infty = F_v^\infty \tag{37}$$

and, as noted earlier, the overstability conditions always reduce to the static instability conditions. Therefore, at the edges, only the gravitational criteria are needed. This shows that at the edges, fingering and diffusive instabilities only occur when a density inversion does.

From Eq. (27) and (30) with w=0, plus some factoring, it can be shown that

$$G_m^\infty = [H_1 p_2 + H_2 q_2]\Delta c_1 + [H_1 q_1 + H_2 p_1]\Delta c_2 = \left[\frac{H_1 q_1 + H_2 p_1}{p_1}\right][q_2 \Delta c_1 + p_1 \Delta c_2] < 0 \tag{38}$$

independent of signs, and that

$$G_v^\infty = \frac{\Delta c_2}{\Delta c_1} \lessgtr \frac{[(A-Z) - \frac{2H_2}{H_1} D_{21}]}{[(A+Z)\frac{H_2}{H_1} + 2D_{12}]} = \frac{2D_{21}}{A+Z} = \frac{A-Z}{2D_{12}} \tag{39}$$

depending on signs. Note that at the onset of instability at the edges (equality signs in Eq. (38) or (39)), $\Delta c_2/\Delta c_1$ depends only on the D_{ij}, and <u>not</u> on density derivatives.

At the center, Eq. (27) and (30) yield the static-diffusive conditions

$$G_m^o = [H_1(\frac{s_1}{s_2}p_1+p_2) + H_2q_2(1-\frac{s_1}{s_2})]\Delta c_1 + [H_1q_1(1-\frac{s_1}{s_2}) + H_2(p_1+\frac{s_1}{s_2}p_2)]\Delta c_2 < 0 \quad (40)$$

independent of signs, and

$$G_v^o = \frac{\Delta c_2}{\Delta c_1} \lessgtr - \frac{[D^{1/2} + D_{22} - \frac{H_2}{H_1}D_{21}]}{[D^{1/2} + D_{11} - \frac{H_1}{H_2}D_{12}]} \cdot \frac{H_1}{H_2} \quad (41)$$

depending on signs. Similarly, Eq. (32) and 35) yield

$$F_m^o = [F_A(\frac{s_1}{s_2}p_1+p_2) + F_B\, q_2(1-\frac{s_1}{s_2})]\Delta c_1 + [F_Aq_1(1-\frac{s_1}{s_2}) + F_B(p_1+\frac{s_1}{s_2}p_2)]\Delta c_2 < 0 \quad (42)$$

independent of signs, and after some algebra

$$F_v^o = \frac{\Delta c_2}{\Delta c_1} \lessgtr \frac{[D_{22} + D^{1/2} - D_{21}\frac{f_2}{f_1}]}{[D_{11} + D^{1/2} - D_{12}\frac{f_1}{f_2}]} \cdot \frac{f_1}{f_2} \quad (43)$$

depending on signs. Here

$$f_1 = \frac{H_2}{H_1}\frac{D_{21}}{D_{11}} - \frac{D_{22}}{D_{11}} \quad (44)$$

$$f_2 = \frac{D_{12}}{D_{11}} - \frac{H_2}{H_1} \quad (45)$$

In this form, Eq. (43) is similar in structure to Eq. (41). Clearly, the static-overstable and fingering conditions are different at the center.

If both cross-terms are zero, then the equations are much simpler. With various known positive factors deleted, we have at the edges

$$G_m^{\infty} = H_2 D_{11}^{1/2} \Delta c_2 < 0 \qquad (D_{12} = D_{21} = 0) \tag{46}$$

and at the center

$$G_m^{o} = H_1 D_{22}^{1/2} \Delta c_1 + H_2 D_{11}^{1/2} \Delta c_2 < 0 \qquad (D_{12} = D_{21} = 0) \tag{47}$$

$$F_m^{o} = H_1 D_{22}^{3/2} \Delta c_1 + D_{11}^{3/2} \Delta c_2 < 0 \qquad (D_{12} = D_{21} = 0) \tag{48}$$

If the H_i are positive, these equations yield the forms of Huppert and co-workers.[9,14]

3. SOME IMPLICATIONS OF THE INSTABILITY CRITERIA FOR FREE DIFFUSION

Contrary to what might be thought, both static-overstable instability at the edges and fingering instability at the center can be experimentally observed with <u>both Δc_i positive</u>. Eq. (42) suggests that a large positive cross-term will give rise to fingering in the center, and Eq. 39 that a large negative one will give static-overstable instability at the edges for positive Δc_i. These conclusions are confirmed by the real systems Bu_4NBr-KBr-H_2O[18] and $ZnCl_2$-KCl-H_2O,[25] respectively.

We have applied Eq. (32) - (48) to various artificial and experimental systems in the region where $S_m > 0$ i.e., where the solution is stable against overturn, and the following have been found. First, whenever Δc_1 and Δc_2 are such that there is instability at the edges of the boundary, the center of the boundary is stable against both fingering and density inversion (i.e., $G_m^o \geq 0$, $F_m^o \geq 0$). If $\Delta c_2/\Delta c_1$ goes deep enough into the instability region, the solution overturn condition is

reached. Second, whenever Δc_1 and Δc_2 are such that there is fingering or density inversion at the center, the edges of the boundary are stable (i.e., $G_m^\infty = \sigma_1 F_m^\infty \geq 0$). Third, as instability is approached at the center in a series of systems with different $\Delta c_2/\Delta c_1$, the fingering instability is always reached first. When $\Delta c_2/\Delta c_1$ goes sufficiently deep into the fingering region, the static-diffusive condition is reached, and when still further, the solution overturn condition is ultimately reached. Thus, at or within the composition region of instability at the center of the boundary, $F_m^o < G_m^o < S_m$; and in addition if $S_m \geq 0$, then $G_m^\infty \geq 0$ also.

If the system is sufficiently unstable from either cause, of course the whole boundary can be completely destroyed in time. Actually, if the compositions are such that static instability is predicted at the center, then fingering convection should have already destroyed the center of the boundary. Consequently, the static condition at the center should have no experimental consequences. It is expected and experimentally found that the deeper one goes into either instability region, the larger are the disturbances until the entire boundary is affected and ultimately completely destroyed (see plates 1 and 2).

It is found from the theory that the onset compositions at the edges depend only on D_{ij}, and at the center on D_{ij} and H_i as well. The actual numerical values of D_{ij} and H_i determine the extent of the stable and unstable regions, and which type of instability is reached first on the diagrams described below.

3.1 Visualization Methods

Although convenient in many theoretical cases, diagrams in terms of dimensionless variables are less convenient in experimental situations. In particular, the characteristic length is ill defined, and there is no exact tie to experimental conditions. For free diffusion boundary conditions we suggest two alternatives, "criteria vs. Δc_1 plots" and a "clock-like diagram".[5] As noted earlier, for free diffusion at any given composition ratio, the largest or smallest value of each instability criterion is either at the center or at the edges of the boundary. Consequently, only those lines need be drawn.

On a criteria plot (CP), the numerical value of each instability criterion can be plotted as a function of both Δc_i in a 3-dimensional plot. A more convenient 2-dimensional way is to plot them as a function of a normalized Δc_1 with proper regard to sign. The normalized Δc_1 is

$$\frac{\Delta c_1}{|\Delta c_1|+|\Delta c_2|} \tag{49}$$

and runs from 0 to 1 or 0 to -1. In Figs. 1-3 are the CP plots for our $SrCl_2$-NaCl-H_2O system using the experimental D_{ij} and H_i given in Table I. All criteria have been scaled by multiplying all D_{ij} by 10^5. On each diagram are lines representing the criteria functions S_m, G_m^∞, F_m^∞, G_m^o and F_m^o of Eq. 2, 38, 36, 40, and 42 respectively. If the Δc_1 fraction of a system is marked as a point at ordinate 0, then the system will be stable to any process whose criterion line is above the point and unstable to any process whose criterion line is below it. The point of onset of an instability is where its criterion line crosses the zero ordinate, and the distance below zero is a normalized measure of how deep into instability the system is. If more than one instability is possible, the lowest (most negative value) is the controlling one.

Fig. 1, with both Δc_1 positive, has all lines above 0. Therefore, for this system, all positive Δc_1 combinations are stable to solution overturn, fingering, and overstability, so the graph is labeled a stable region. As noted earlier, there are other systems whose diagrams have lines going below zero even when both Δc_1 are positive.

Fig. 2, with Δc_1 negative and Δc_2 positive, has a small stable region, and is most stable at $\Delta c_1=0$. As the Δc_1 fraction becomes more negative, F_m^o (fingering at center) crosses zero first, followed by G_m^o, and then S_m. Consequently, fingering can occur even if the system is gravitationally stable at the center and edges. Even as solution overturn is approached, the system does not first become unstable at the edges. Because fingering appears first when starting from a stable region, this graph is labeled a fingering region.

Fig. 3, with Δc_1 positive and Δc_2 negative, shows a stable region and is most stable at a Δc_1 fraction of 1 ($\Delta c_2=0$). In going from stable to unstable (Δc_1 decreasing), the G_m^∞ and F_m^∞ lines cross zero first, and at the same point. Therefore, the static-overstable instability at the edges starts first, and the graph is so labeled. Even as solution overturn is approached, fingering or static instabilities at the center do not come first. Eq. 36 requires the G_m^∞ and F_m^∞ lines to cross at zero ordinate. (The diagram for both Δc_1 negative is not shown here, but the system is unstable everywhere because all lines are below zero.)

The clock-like diagram (CLD) has the advantage of containing all the experimental conditions on a single plot, and shows the boundary lines, regions of instability, and relations among the regions more clearly than a set of CP diagrams. Its disadvantage is that a quantitative measure of each

instability cannot be shown. A CLD has the concentration of the slower moving component c_1 as the abscissa and the faster moving one c_2 as the ordinate. Fig. 4 is the CLD for our $SrCl_2$-NaCl-H_2O system.

On a CLD, the average composition of the system is a center of symmetry for the compositions of the corresponding top and bottom solutions. The lines on this diagram indicate the $\Delta c_2/\Delta c_1$ ratios at the onset of the instabilities and are obtained from equality signs in Eq. 3, 39, 41, 43 for S_v, $G_v^\infty = F_v^\infty$, G_v^o, and F_v^o respectively, or from zero values of S_m, G_m^∞, G_m^∞, and F_m^o, respectively.

Line N (S_v, Eq. 3) indicates compositions of neutral density (solution overturn). Bottom solutions lie above it and top solutions below it when H_1 and H_2 are positive. If both are negative, the opposite is true. If either H_1 or H_2 is negative, the higher density solutions lie on the side for which c_1 or c_2 respectively is smaller.

Line G ($G_v^\infty = F_v^\infty$, Eq. 39) is the onset line for static/overstable/finger instabilities at the edges of the boundary. These instabilities appear for top and bottom solutions whose compositions lie between lines G and N.

Line F (F_v^o, Eq. 43) is the onset line for fingering at the boundary center. These instabilities appear for top and bottom solution compositions between lines F and N.

Line D (G_v^o, Eq. 41) is the onset line for static-diffusive instabilities at the boundary center. The compositions of solutions between D and N would be statically unstable. The D line always lies between F and N, so that there is a region between F and D which is density stable but fingering unstable.

Line R is the isorefractometric line, along which the refractive index of top and bottom solutions is the same. This line, not related to instabilities,

tells the experimenter where there will be the same number of Gouy fringes on each side of the undeviated slit image. (The ones above are "negative" fringes, so that $J_m = 0$).

3.2 Effects of Changing D_{ij} and H_i

The slopes of CLD lines depend on the values of D_{ij} and H_i. However, all free diffusion CLD are topologically similar to Fig. 4 or its mirror image about a vertical or horizontal line. The field of instabilities always lies in that area between lines F and G which contains line N. Stable boundary compositions lie in that area between F and G which does <u>not</u> contain N. Some general features of CLD's are indicated on Fig. 5. The quantities

$$P_1 = D_{11} + (H_2/H_1)D_{21} \tag{50}$$

$$P_2 = D_{22} + (H_1/H_2)D_{12} \tag{51}$$

and the inequality

$$P_1 \begin{matrix} \leq \\ \geq \end{matrix} P_2 \tag{52}$$

will be useful. Eq. 50 and 51 are related to the $\Gamma_+^{(1)}$ and $\Gamma_-^{(1)}$ used by Vitagliano et al.[5]

Consideration of the effects of changing D_{ij} and H_i yields the following results.

(a) Changing the sign of H_2/H_1 reverses the fingering and overstability fields with respect to line N, as shown in Fig. 5A and B. The G line is invariant since G_v^∞ is independent of H_1 and H_2 by Eq. 39.

(b) Changing the signs of H_2/H_1, D_{12}, and D_{12} transforms the CLD into its mirror image with respect to a vertical or horizontal line through the center of symmetry.

(c) Increasing D_{12} and/or decreasing D_{21} turns the F line clockwise and the G line counterclockwise, as shown by the arrows on Fig. 5C. With appropriate values, the F or G lines may have a positive slope; in these cases instabilities can occur when both Δc_i are positive.

(d) For $P_1<P_2$ and $H_2/H_1>0$, as shown in Fig. 5A or C, the composition region of fingering instability is clockwise from N to F and of overstability is counterclockwise from N to G. For $P_1>P_2$ and $H_2/H_1>0$, the composition regions reverse as shown on Fig. 5C.

(e) If $P_1=P_2$ both the F and G lines fall on top of the N line, and the diffusion system is stable for any $\Delta c_2/\Delta c_1$ ratio. In this circumstance, $\Gamma_+(\rho)$ and $\Gamma_-(\rho)$ of the diffusion equations (Ref. 5, Eq. 19, 20) are independent of Δc_1 and Δc_2.

(f) For D_{22} much larger than D_{11}, the F line approaches an infinite slope (vertical) and the G line a zero slope (horizontal). This is analogous to the heat-salt situation where the thermal diffusivity is 100 times the mass diffusivity.

An alternate CLD is the plot of $\Delta\rho_2$ vs $\Delta\rho_1$. In this representation, the N line is invariant to changes in H_1 and H_2 and its slope is always -1.

It is also instructive to examine the density profiles which would be induced by diffusion if convection were inhibited. As $\Delta c_2/\Delta c_1$ ratios approach the solution overturn ratio, the diffusion equations predict the shapes shown in Figure 6. The fingering situation is indicated by sketches 1-5. Sketch 1 corresponds to the onset of fingering at the center; sketch 2 shows a multiple inflection point and corresponds to the fingering situation between lines F and D in a CLD, even though the density is monotonic with X. When the slope at the center is horizontal, as in sketch 3, this corresponds

to line D, the onset of static instability. Sketch 4 is further in, and there is a clear density inversion at the center. Finally sketch 5 is the solution overturn case. Sketches 6-9 indicate the profiles for the static-overstable situations at the boundary edges. Sketch 6 corresponds to the onset of overstability. Sketches 7 and 8 are in the overstable region as can be seen by the maxima and minima at the edges. Finally sketch 9 corresponds to solution overturn; it is the reverse of sketch 5.

4. EXPERIMENTAL

4.1 Materials and Compositions

We have primarily used the system $SrCl_2$(0.5 M)-NaCl(0.5 M)-H_2O, which has significant cross-term D_{ij}. The concentrations are high enough so that Δc_i of 0.2 do not significantly change the values of D_{ij}, but are not so concentrated as to use large amounts of highly purified materials. Densities and diffusion coefficients are given in Table I, with details to be reported elsewhere.[19] In Table II are the border compositions for the onset of instabilities. In Table III are the Δc_1 and Δc_2 for a series of experiments from stable to nearly solution overturn for both the fingering and overstable regions. One experiment was done for $ZnCl_2$(0.5)-KCl(4.0)-H_2O previously observed at LLNL to be unstable at the edges even though Δc_i are both positive.

Preparation and sources of materials are described elsewhere.[26,27,28] Solutions were prepared by weight, using analyzed stock solutions of $SrCl_2$ and $ZnCl_2$ and dried samples of NaCl and KCl. The water was deionized, then distilled once.

4.2 Optical Techniques

Optical methods are best to observe the instabilities because the convective motions cause light beams to deviate both in vertical and horizontal planes. The shadowgraph technique has been widely used for large scale experiments with wide boundaries.[1,2,9,14] However, the narrow boundaries of free diffusion are difficult to visualize by this technique. Consequently, we have explored the schlieren and interferometric methods used in measuring diffusion coefficients.[24] The high precision Gosting diffusiometer,[29] now at LLNL, has a simple Gouy and Rayleigh optical system whose images are photographed on 4 in x 5 in films or plates. It can be converted to the astigmatic Philpot-Svensson Schlieren system[30-35] by the addition of other optical components at and beyond the usual focus of the Gosting diffusiometer. These additions give a smaller image which can be captured on 35 mm film (Kodak Panatomic IS032.)

The simple Gouy and Rayleigh optics average over each horizontal plane in the cell, and do not really show the instabilities which cause variations in refractive index in such a plane. The simple Rayleigh does show some average composition differences as well as light thrown out of the diffraction pattern, but the results are less satisfying than those from the Philpot-Svensson arrangement. Simple Gouy and Rayleigh photographs taken on Royal Pan film are not reported here.

Our Philpot-Svensson arrangement is shown in Figure 7. There is a light source slit LS, which is focused by the main lens SL onto the schlieren plane (SP) (the photographic plane of the usual Gosting diffusiometer arrangement). The converging light passes through a mask M (two vertical slits for Rayleigh, one for other arrangements), and then through the cell containing the boundary. For schlieren pictures, a diagonal slit or phase plate is placed at

the schlieren plane. Beyond it is a camera lens CL which focuses the cell C on the photographic plane (PP). Beyond the camera lens is a cylinder lens CY which focuses the image at the SP onto PP.

With this Philpot-Svensson system, there are five arrangements of the components which could indicate refractive index anomalies caused by convective motions. These differ in the orientation of the source slit or cylinder lens, and in the number of slits in the cell mask. We found three of them to be particularly useful; Gouy, (G) "single slit Rayleigh" (SSR) and schlieren (S).

(1) Gouy.

In this "modified" Gouy, the source slit and cylinder lens are both horizontal and a single cell mask slit is used. The usual Gouy image at SP shows no evidence of fringe distortion. However, the cylinder lens, which refocuses this image onto PP, uncouples the horizontal averaging if there are refractive index disturbances along a horizontal plane in the cell. Therefore, convective motions give rise to distorted Gouy fringes. Outer Gouy fringes are primarily formed from effects in the central portion of the boundary, and inner fringes from the combined effects of the two outer portions (edges) of the boundary. Consequently, observing which fringes are distorted give an excellent characterization of the location and extent of the disturbances. However, there is not a 1-1 correspondence of cell level with fringes, since both sides of the interface contribute to each fringe (and wave theory shows that every part of the solution contributes a small amount to each fringe.)[36] This technique was found to give the most sensitive measure of the instabilities. It is a little more tedious experimentally than the others because the source slit width and exposure times must be decreased as the fringe pattern shrinks with time.

(2) Schlieren

Here the source slit remains horizontal, but the cylinder lens is vertical. A diagonal line from a phase plate at SP intercepts the light deviated by the cell boundary. This light forms an image at PP of the vertical refractive index gradient in the cell. Each point on this image is the derivative averaged horizontally at a corresponding level across the cell, but does not show individual horizontal convective disturbances at that level. However, if disturbances are large enough, the average will be effected and the shape of the overall gradient curve will change irregularly with time. This technique works best for the overstability case, but is not as sensitive as the modified Gouy.

(3) Rayleigh

For Rayleigh, a second slit in the cell mask is used over the reference arm of this interferometer (here the water of the thermostat bath). The source slit and the cylinder lens are both vertical. The fringes could not be resolved by the Panatomic film at early times. Moreover, they result from a horizontal average across the cell at each level, and do not show individual convective disturbances. For sufficiently large disturbances, the Rayleigh patterns show unusual changes with time, but are less sensitive than the Gouy. Some light is deviated from the diffraction pattern by horizontal refractive index variations, but the effect is better seen in the following arrangement.

(4) Single Slit Rayleigh

This arrangement is the same as the Rayleigh except only the cell mask slit over the cell is used. In stable diffusing systems, a long blurred rectangular image of the cell is observed,[35] because any light deviated downwards by the boundary is swamped by the undeviated light. However, in the

presence of refractive index variations along a horizontal line, light is deviated horizontally. At the camera, these deviations can appear as distortions of the rectangle or even as blotches on either side of a fuzzy image. This technique is quite sensitive, especially for the fingering situation. It also corresponds well to a one-to-one correspondence between cell level and image level.

(5) Vertical Schlieren

A schlieren arrangement in which the source slit is vertical and the cylinder lens horizontal was suggested by Prof. G. Kegeles[37] in a different context.[38,39] This averages along vertical planes in the cell, and will indicate the derivative of refractive index in the horizontal direction. This should indicate finger instabilities. However, finger images at a particular level in the boundary will be swamped unless the large uniform regions of the cell are masked off. This requires a vertically movable, narrow horizontal mask, which was not available for this research. This technique should be explored in future work.

Table 2 summarizes these configurations where G, S, R, SSR, and VS refer to modified Gouy, Schlieren, Rayleigh, "single slit Rayleigh", and vertical schlieren. H and V refer to horizontal and vertical positions of the source slit or cylinder lens.

In stable systems, our Philpot-Svensson Gouy and Rayleigh images look the same as the corresponding ones from the simple arrangement but are smaller. In unstable systems, the Philpot-Svensson Rayleigh fringes still look the same as their simple counterparts, but the "modified Gouy" fringes show distortion. So do single slit Rayleigh patterns, and to a somewhat lesser extent so do schlieren. The effectiveness of these last three can be seen in the accompanying plates 1-6.

The added Philpot-Svensson optical parts consisted of a Schlieren phase plate from an electrophoresis apparatus, a Perkin-Elmer spherical lens from an earlier University of Wisconsin diffusiometer (focal length ~75 cm), a Continental Optics 1/4 wave cylinder lens (focal length ~20 cm), and a Zeiss Rolleiflex 35mm camera with lenses removed. The cylinder lens was mounted on a Klinger rotation stage which allowed a rapid change back and forth from horizontal to vertical. These were mounted on riders with screw or micrometer mounts to aid in accurate positioning. Positioning and final focusing at PP were done with the aid of a Zeiss alignment telescope, using the sharpest Rayleigh fringes from a sharp boundary for the camera lens and best image of the horizontal LS slit at SP for the cylinder lens. The emulsion plane of the camera was located at PP, the combined camera and cylinder lens focus.

The light source was a 100 watt AH4 Hg lamp, with the blue line removed with a Wratten 77A filter. Some initial pictures show an unwanted red line at the undeviated slit image, which was subsequently eliminated by the addition of a Wratten 52 filter. The cell was a Beckman glass Tiselius cell whose reference arm for Rayleigh is the water of the water bath. The cell was filled using standard techniques.[24,40]

The boundary sharpening technique consists of a long needle at the optic axis through which top and bottom solutions flow out. At the start of the run, a stopcock is closed, and the needle pulled out. This technique is quite satisfactory, but there should be less initial boundary distortion if the boundary were sharpened from the side using a more complex cell with a side slit.[24]

5. Results and Discussion

The optical results of our experimental runs in stable and unstable regions are shown on Plates 1-6. Our experimental conditions, given in Table III and on Figs. 1-3, are best shown on the CLD, Fig. 4.

As noted in the previous section, stable boundaries have a ladder-like undistorted set of Gouy fringes (Plate 1.1) and a rectangular SSR image (Plate 4.5). Moderate boundary disturbances at the center distort the outer (lowest) Gouy fringes and leave the inner ones undistorted (Plate 1.4); in the SSR image, light is deviated at the center (Plate 3.6). Moderate disturbances at the edges distort the inner Gouy fringes, and leave the outer ones undistorted (Plate 2.4); in the SSR image, light is deviated at the boundary edges (Plate 4.7).

Plate 1 contains sets of Gouy fringes for a series of systems whose compositions start in the stable region and go into the fingering instability region. The stable boundary picture 1.1 exhibits the expected unperturbed horizontal fringes throughout the whole pattern. Picture 1.2 corresponds to run 2 which is just inside the onset of fingering (line F) but is density stable. The outer three or four fringes are distorted, indicating a disturbance at the center as predicted by theory. Runs 3-5 are increasingly deeper in the statically stable, fingering unstable region; and the corresponding pictures 1.3-1.5 show the distortion of fringes spreading inward (upward) until the whole pattern is distorted in picture 1.5. The distortion is still worse in run 6 (picture 1.6) which would also be statically unstable at the boundary center. This plate neatly verifies (1) that boundary instabilities can occur at the boundary center even if the systems are statically stable, and (2) that the instabilities are visible just inside the onset line predicted by McDougall's theory.

Plate 2 contains sets of Gouy fringes for systems whose compositions start in the stable region and go into the static-overstable instability region. It can be shown from Eq. 39 that inversions of concentration, density, and refractive index appear at the same $\Delta c_2/\Delta c_1$ ratio at the boundary edges. Consequently, fringes will appear above the undeviated slit image, as well as below. These "negative" upper fringes correspond to the edges of the boundary, and therefore should show any perturbations there. Picture 2.1 is the stable, undistorted case. Picture 2.2 (run 11) shows a slight distortion of the uppermost fringe, all others being undistorted. Pictures 2.3 (run 10) and 2.4 (run 9) are increasingly deeper into the instability region, and only the outer fringes (corresponding to the boundary center) are undistorted. Pictures 2.5 (run 8) and 2.6 (run 7), still more unstable, show disturbances throughout the entire pattern. These results are consistent with theory, but it was not possible to see distortion close to the overstability onset line G. It is necessary to go deeper into the overstability field than into the fingering field to see convection.

Plate 3 contains sets of Gouy and SSR pictures taken at nearly corresponding times during the course of run 6 (deep in the fingering region). Plate 4 contains similar sets taken during the course of run 8(deep in the overstable region). Both plates clearly show substantial changes in the shapes of the Gouy fringes with time, indicating the irregular growth of convective motions. The SSR on plate 3 shows that an initial modest fingering perturbation grows with time until it ultimately obliterates the boundary. In contrast, the SSR on plate 4 shows that an initial distortion at the edges becomes weaker with time, and the center becomes a little more regular. Boundary perturbations are still visible at some distance from the center. We note that the fingering effects spread throughout the boundary more rapidly

than do the overstable ones, as shown by the SSR pictures and by the fact that the fingering Gouy pattern shrinks more rapidly than the overstable Gouy pattern.

Plates 5 and 6 contain schlieren patterns for the fingering and overstable cases respectively. The runs must be deep inside the convection field before schlieren patterns show any effects. Since schlieren patterns show the gradient of refractive index, the patterns of plate 5 would show two maxima and a deep minimum at the center in the absence of convection. Convection destroys this appearance, and only one maximum is observed. However, the pattern is irregular and changes shape with time. Small perturbations along the base line are evidence of convective motion through the top and bottom solutions.

Plate 6 is more impressive. The refractive index (and density) inversion at the edges of the boundary are clearly evident. Convective motion at the edges is shown by the irregular changes in the patterns with time, e.g., the extra "horns" which appear and disappear. The disappearance of convection at the center after long times is evident in picture 6.6.

Our one experiment with $ZnCl_2$ (0.5M)-KCl(4M)-H_2O was predicted to be unstable at the edges with positive ΔC_1, and indeed gave Gouy photographs (not shown) with slight curvature in the innermost fringes quite similar to picture 2.2.

Our experiments involve an isothermal ternary system with significant cross terms which undergoes free diffusion. We conclude that these experiments accurately verify McDougall's theory for the onset of the fingering instability at the center of the boundary. As predicted, this instability first occurs for compositions where the system is statically stable. Our experiments are consistent with the predictions of McDougall's

theory in the overstable region at boundary edges, but it has not been possible to detect instabilities as close to the point of onset as was the case for fingering.

We suggest the following for future work. First, a more systematic variation of Δc_1 for the same $\Delta c_2/\Delta c_1$ ratio to see if the numerical values of G_m^∞ and F_m^o can be correlated with the onset of convection. For example, in an additional run with Δc_1 at one-fourth the value in Table III, convection was not observed. Second, a cell with a side slit for sharpening would improve the initial boundary. Third, a movable horizontal mask with vertical schlieren should be explored as a detection technique.

This work was performed under the auspices of the U. S. Department of Energy by the Lawrence Livermore National Laboratory under contract W-7405-Eng-48. We are grateful to Dr. R. N. Schock and the LLNL Earth Sciences Division for support of VV, to OBES Geosciences for support of DGM, and to Sue Frumenti for the word processing of the manuscript.

The permanent address of VV is the Dipartimento di Chimica Via Mezzocannone 4, Universita di Napoli, 80134 Naples, Italy.

TABLE I. Properties of $SrCl_2$-NaCl-H_2O[a]

$\bar{c}_1$	0.5	$10^5 D_{11}$	0.9980
$\bar{c}_2$	0.5	$10^5 D_{12}$	0.1142
H_1	0.132650	$10^5 D_{21}$	0.2975
H_2	0.038141	$10^5 D_{22}$	1.2310
R_1	2441.8		
R_2	856.2		

a Units are $\bar{c}_i$ in mol-dm^{-3}, H_i in g-dm^3-mol^{-1}-cm^{-3}, and D_{ij} in cm^2-s^1.

TABLE II. Philpot-Svensson Optical Arrangements

Type	Source	No. of Cell Mask Slits	Phase Plate	Cylinder Lens	Nominal Width of Source Slit (microns)	Exposure Times(s)
Modified Gouy	H	1	not used	H	100-30	12-5
Schlieren	H	1	in	V	100	8 1/2
Rayleigh	V	2	not used	V	30	1 1/4
"Single Slit Rayleigh"	V	1	not used	V	50	2 1/2
Vertical Schlieren	V	1	in	H	-	-

TABLE III. Criteria for System $SrCl_2$(0.5M)-NaCl(0.5M)-H_2O

Type	Δc_1	Δc_2	$\frac{\Delta c_1}{\lvert\Delta c_1\rvert+\lvert\Delta c_2\rvert}$	$\Delta c_2/\Delta c_1$	Description
F	<0	>0	-.081	-11.30	finger border
D	<0	>0	-.179	- 4.60	diffusion instability border
N	-	-	-.223	- 3.48	solution overturn
R	>0	<0	.260	- 2.85	isorefractometric ratio (J_m=0)
G	>0	<0	.526	- 0.90	static-overstability border

TABLE IV. Experimental Runs for $SrCl_2$(0.5M)-NaCl(0.5M)-H_2O

Case	Δc_1	Δc_2	$\frac{\Delta c_1}{\lvert\Delta c_1\rvert+\lvert\Delta c_2\rvert}$	$\Delta c_2/\Delta c_1$	J_m[a]	Description	Plate
1	0.06	0.06	-.071	-13.0	66.8	just inside stable	(not shown)
2	-0.02	0.20	-.091	-10.0	61.3	border of finger	1.2
3	-0.025	0.20	-.111	- 8.0	55.1	finger	1.3
4	-0.033	0.20	-.143	- 6.0	66.8	finger	1.4
5	-0.042	0.20	-.172	- 4.8	34.8	finger	1.5
6	-0.0665	0.20	-.189	- 4.3	28.8	inside diff. inst. (finger region)	1.6
7	0.062	-0.20	+.238	- 3.2	3.3	overstability	2.6
8	0.080	-0.20	+.286	- 2.5	12.0	overstability	2.5
9	0.091	-0.20	+.312	- 2.2	25.6	overstability	2.4
10	0.100	-0.20	+.333	- 2.0	36.7	overstability	2.3
11	0.133	-0.20	+.400	- 1.5	77.2	overstability	2.2
12	0.04	0.04	+.5	+ 1	65.9	stable	1.1, 2.1

[a] J_m is the total number of fringes in the Gouy pattern.

REFERENCES

1. HUPPERT, H. E. & TURNER, J. S., J. Fluid Mech. 106, 299 (1981).

2. TURNER, J. S., Ann. Rev. Fluid Mech. 17, 11 (1985).

3. VITAGLIANO, V., ZAGARI, A., SARTORIO, R. & CORCIONE M., J. Phys. Chem. 76, 2050 (1972).

4. VITAGLIANO, V., SARTORIO, R. & COSTANTINO, L., J. Phys. Chem. 78, 2292 (1974).

5. VITAGLIANO, V. SARTORIO, R., SPADUZZI, D. & LAURENTINO, R., J. Solution Chem. 6, 671 (1977).

6. WENDT, R. P., J. Phys. Chem. 66, 1740 (1962).

7. KIM, H., J. Phys. Chem. 74, 4577 (1970).

8. CHEN, C. F. & JOHNSON, D. H., J. Fluid Mech. 138, 405 (1984).

9. HUPPERT, H. E. & MANINS, P. C. Deep Sea Res. 20, 315 (1973).

10. COMPER, W. D. & PRESTON, B. N. Advances in Polymer Science 55, 105 (1984).

11. COMPER, W. D., CHECKLEY, G. J. & PRESTON, B. N., J. Phys. Chem. 88, 1068 (1984). See also previous articles, ibid. 87, 648, 655, 662, 667 (1983).

12. MCDOUGALL, T. J. & TURNER, T. S., Nature (London) 299, 812 (1982).

13. MCDOUGALL, T. J., J. Fluid Mech. 126, 379 (1983).

14. HUPPERT, H. E. & HALLWORTH M. A., J. Phys. Chem. 88, 2902 (1984).

15. VITAGLIANO, P. L., DELLA VOLPE, C. & VITAGLIANO, V., J. Solution Chem. 13, 549 (1984).

16. TYRRELL, H. J. V., private communication July 1984.

17. MILLER, D. G., in preparation.

18. KIM, H., J. Solution Chem. 3, 149 (1974).

19. RARD, J. A. & MILLER, D. G. (details of $SrCl_2$-NaCl-H_2O system), in preparation.

20. VITAGLIANO, V., BORRIELLO, G. & DELLA VOLPE, C., in preparation.

21. VITAGLIANO, V., SARTORIO, R., SCALA, S. & SPADUZZI, D., J. Solution Chem. 7, 605 (1978).

22. MILLER, D. G., VITAGLIANO, V. & SARTORIO, R., submitted for publication.

23. FUJITA, H. & GOSTING, L. J., J. Am. Chem. Soc. 78, 1099 (1956).

24. DUNLOP, P. J., STEEL, B. J. & LANE, J. E., in "Physical Methods of Chemistry", Vol. 1, Part IV, A. Weissberger and B. Rossiter, Ed., John Wiley and Sons, New York, N. Y., Chap. IV, 1972, p. 207-349.

25. TING, A. W., MILLER, D. G. and RARD, J. A., in preparation.

26. RARD, J. A. & MILLER, D. G., J. Chem. Soc. Faraday Trans. 1 78, 887 (1982).

27 RARD, J. A. & MILLER, D. G., J. Chem. Eng. Data 29, 151 (1984).

28. RARD, J. A. & MILLER, D. G., J. Chem. Eng. Data 25, 211 (1980).

29. GOSTING, L. J., KIM, H., LOEWENSTEIN, M. A., REINFELDS, G., & REVZIN, A., Rev. Sci. Inst. 44, 1602 (1973).

30. PHILPOT, J. S. L., Nature 141, 283 (1938).

31. SVENSSON, H. Kolloid-Z., 87, 181 (1939).

32. SVENSSON, H. Kolloid-Z., 90, 141 (1940).

33. SVENSSON, H. & THOMPSON, T. E. in "Laboratory Manual of Analytical Methods in Protein Chemistry", Vol. 3, P. Alexander and R. J. Block, eds., Pergamon Press N. Y., 1961, pp. 57-118.

34. LONGSWORTH, L. G. Ind. Eng. Chem. Anal. Ed. 18, 219 (1946).

35. LONGSWORTH, L. G. in "Physical Techniques of Biological Research", 2nd ed. Vol. II, Part A, Chap. 3, Academic Press, New York, (1968).

36. TYRRELL, H. J. V. & HARRIS, K. R. 1984 "Diffusion in Liquids", Butterworths, London.

37. KEGELES, G. 1981 private communication.

38. BIANCHERIA, A. & KEGELES, G., J. Am. Chem. Soc. 79, 5908 (1957).

39. TROUTMAN, R. & GOFMAN, J. W., J. Phys. Chem. 56, 464 (1952).

40. WOOLF, L. A., MILLER, D. G. & GOSTING, L. J., J. Am. Chem. Soc. 84, 317 (1962).

Fig. 1

Criteria plot CP for $SrCl_2$(0.5M)-NaCl(0.5M)-H_2O. Instability criteria vs. normalized Δc_1 for $\Delta c_1>0$, $\Delta c_2>0$. All compositions are stable including run 12.

Fig. 2

CP for $SrCl_2$(0.5M)-NaCl(0.5M)-H_2O. Instability criteria vs. normalized Δc_1 for $\Delta c_1<0$, $\Delta c_2>0$. Run 1 is stable; runs 2-5 are statically stable but unstable to fingering at the center; run 6 is statically and fingering unstable.

Fig. 3

CP for $SrCl_2$(0.5M)-NaCl(0.5M)-H_2O. Instability criteria vs. normalized Δc_1 for $\Delta c_1>0$, $\Delta c_2<0$. Runs 7-11 are in the composition region for static-overstable instability at boundary edges.

Fig. 4

CLD for the system $SrCl_2$(0.5M)-NaCl(0.5M)-H_2O at 25°C.

Line F: Onset line for appearance of fingers at boundary center (F_m^o=0).

Line D: Onset line for static instability at boundary center (G_m^o=0).

Line N: Neutral density or solution overturn line (S_m=0).

Line R: Isorefractometric line (J_m=0, with same number of fringes above and below undeviated slit image).

Line G: Onset line for static-overstability at boundary edges (G_m^∞=0).

The numbers 1-12 indicate the compositions of top and bottom solutions for all our runs. For numerical values see Table II.

Fig. 5

Sketches of the "clock-like diagrams" CLD for various D_{ij} and H_2/H_1 conditions showing composition regions for stable and unstable boundaries.

(1) Instability conditions at the center of the boundary (fingers).

(2) Instability conditions at the edges of the boundary (overstability).

(F) Limiting slope for fingers at center (F_m^o=0 or Eq. 43).

(D) Limiting slope for density inversions at center due to diffusion (G_v^o=0 or Eq. 41).

(N) Neutral density line (S_m=0 or Eq. 3).

(G) Limiting slope for overstability at edges (G_m^∞=0 or Eq. 39).

Fig. 6

Density distribution through diffusion boundary in a ternary system for various $\Delta c_2/\Delta c_1$ conditions if convection were inhibited.

(1) Density profile corresponding to onset of finger instability at boundary center.

(2) Density profile for fingering instability, $\Delta c_2/\Delta c_1$ conditions in center between lines F and D of figure 4.

(3) Profile at $\Delta c_2/\Delta c_1$ given by line D of figure 4.

(4) Profile for $\Delta c_2/\Delta c_1$ compositions between lines D and N of figure 4.

(5) Profile at neutral density line (solution overturn), line N.

(6) Profile at onset of overstability at edges of the boundary (line G of figure 4).

(7-8) Profile for overstability at edges, $\Delta c_2/\Delta c_1$ conditions between lines G and N of figure 4.

(9) Profile at neutral density line (line N of figure 4); same as graph 5 with top and bottom solutions reversed.

The graphs of density gradients through the boundary corresponding to graphs 1, 2, 3, 4, and 6, 7, 8 can be seen in Ref. 5: Fig. 3 graphs B, 3, 4, 5, and A, 2, 1 respectively.

Fig. 7

Philpot-Svensson Optical System, with light source (LS), schlieren lens (SL) cell mask (M), Tiselius cell (C), schlieren plane (SP), camera lens (CL), cylinder lens (CY), and photographic plane of focus (PP).

Plate 1

Comparison of modified-Gouy fringes from a stable composition (run 12) with compositions going increasingly deeper into the finger instability region at the boundary center (runs 2-6). Run 6 is also statically unstable.

Pictures 1-6 are respectively: Run 12 (stable) at 17'; Run 2 at 8'; Run 3 at 10'; Run 4 at 4.3'; Run 5 at 4'; Run 6 at 5'.

For $\Delta c_2/\Delta c_1$ data see Table II.

Plate 2

Comparison of modified-Gouy fringes from a stable composition (run 12) with compositions increasingly deep in the static-overstability region at the boundary edges (runs 7-11).

Pictures 1-6 are respectively: Run 12 (stable) at 17'; Run 11 at 3'; Run 10 at 10'; Run 9 at 11'; Run 8 at 11'; Run 7 at 33'.

For $\Delta c_2/\Delta c_1$ data see Table II.

According to Eq. (39), which shows $\Delta c_2/\Delta c_1$ is independent of the H_2/H_1 ratio, a refractive index inversion, as well as a density and a concentration inversion, appears at the edges of the boundary. Therefore, Gouy fringes can be seen on both sides of undeviated light. As the compositions approach the isorefractometric line, the number of upward fringes increases with respect to that of downward ones.

Plate 3

Gouy and SSR pictures for Run 6 (fingers). $\Delta c_2/\Delta c_1=-4.3$ at different times. Pictures 1-5: 5', 11.4', 17', 23', 47'; 6-10: 2.5', 9', 15', 21', 45'.

Plate 4

Gouy and SSR pictures of Run 7 (overstability). $\Delta c_2/\Delta c_1$=-2.5 at different times. Pictures 1-4: 5', 11', 17', 33'; 6-9: 3', 9', 15', 31' 5: Picture Run 12 (stable boundary), 21'.

Plate 5

Schlieren pictures of Run 6 (fingers). $\Delta c_2/\Delta c_1$=-4.3 at different times. Pictures 1-4: 4', 10', 15', 32'.

Plate 6

Schlieren pictures of Run 7 (overstability). $\Delta c_2/\Delta c_1$=-3.2 at different times. Pictures 1-6: 10', 16', 31', 46', 63', 136'.

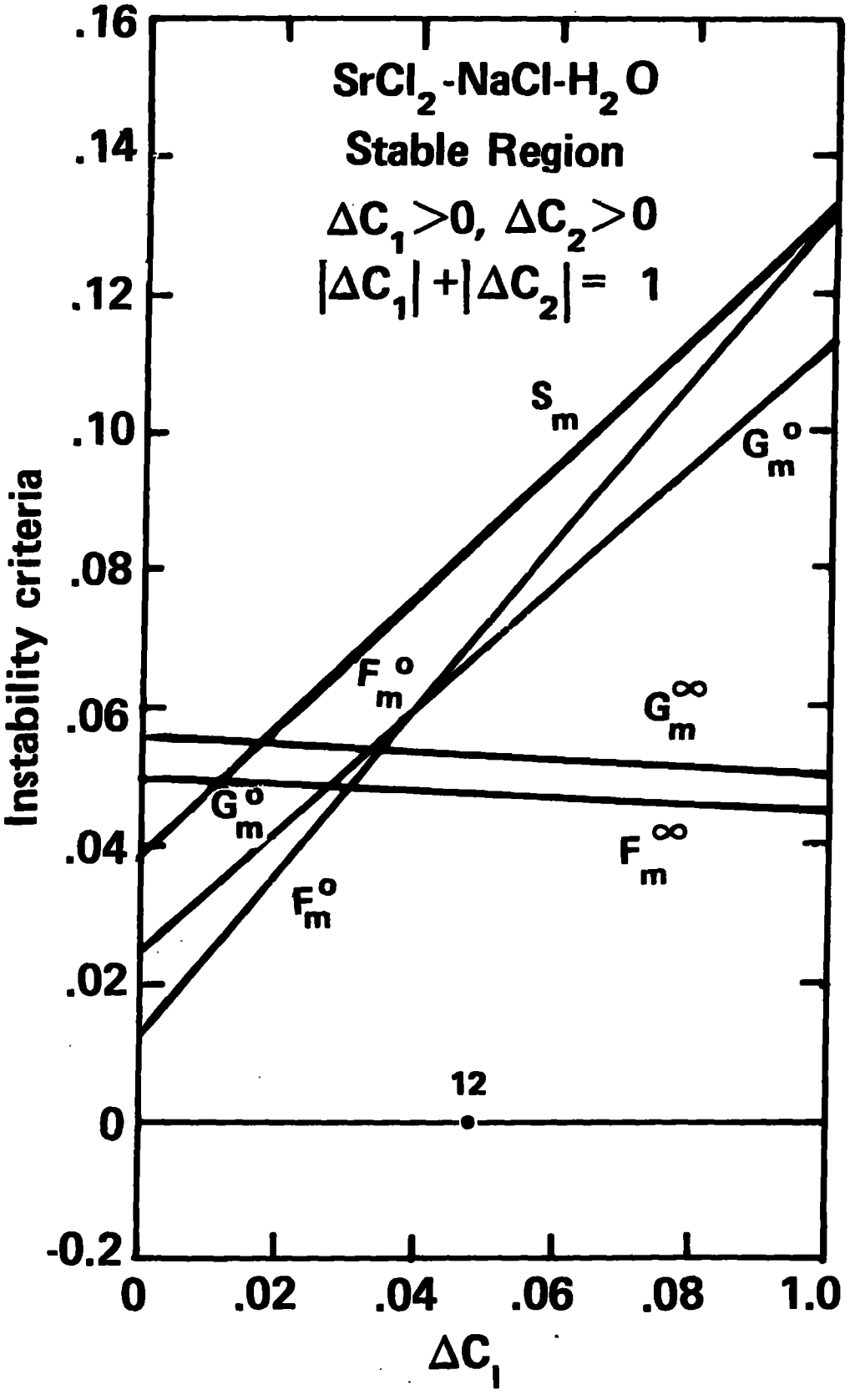
$SrCl_2$-NaCl-H_2O
Stable Region
$\Delta C_1 > 0$, $\Delta C_2 > 0$
$|\Delta C_1| + |\Delta C_2| = 1$
S_m
G_m^o
F_m^o
G_m^∞
G_m^o
F_m^∞
F_m^o
12
Instability criteria
.16
.14
.12
.10
.08
.06
.04
.02
0
-0.2
0
.02
.04
.06
.08
1.0
ΔC_1

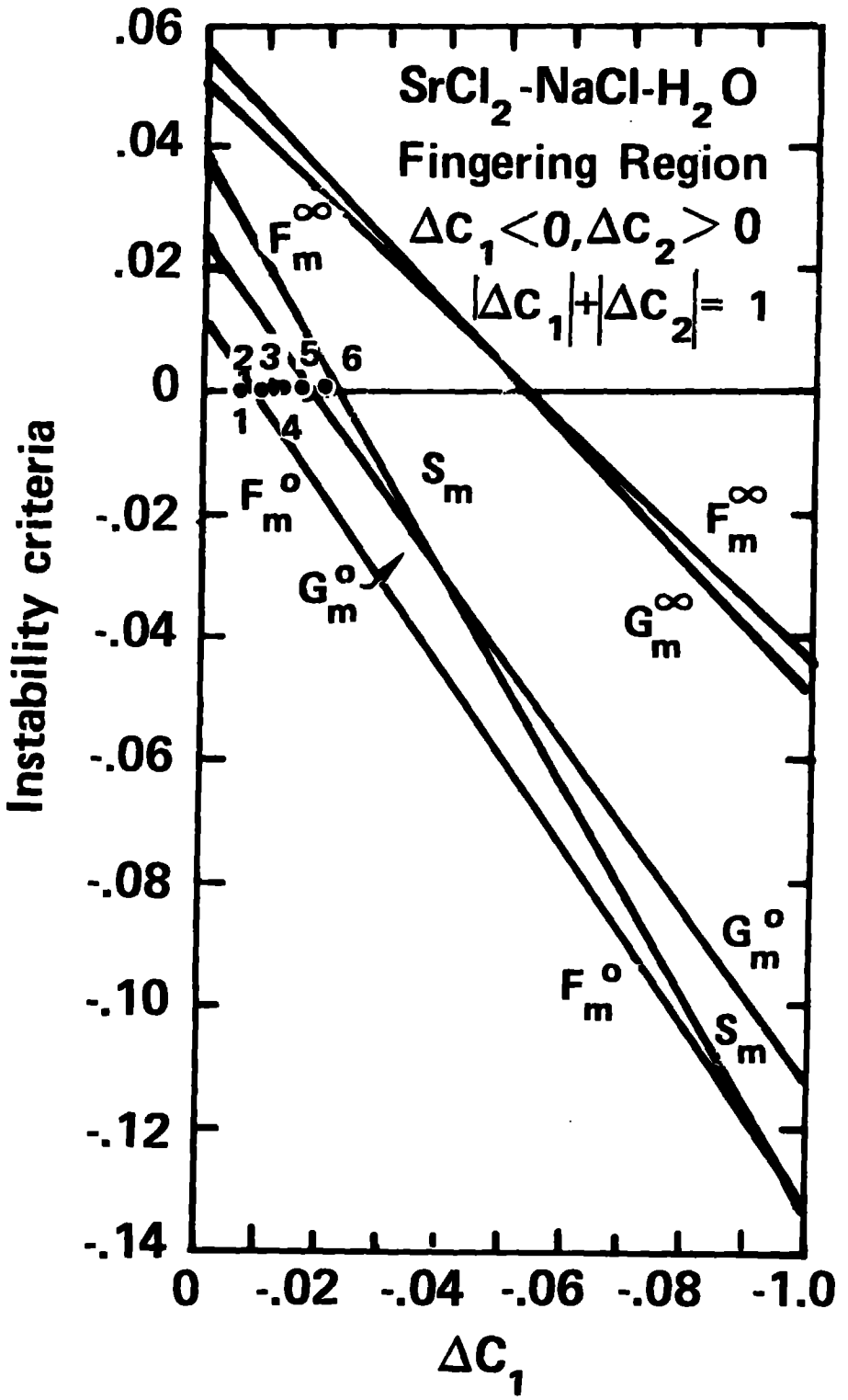
.06
.04
.02
0
-.02
-.04
-.06
-.08
-.10
-.12
-.14
Instability criteria
SrCl2-NaCl-H2O
Fingering Region
ΔC1<0, ΔC2>0
|ΔC1|+|ΔC2|= 1
F∞m
F°m
S m
G°m
G∞m
1
2
3
4
5
6
0
-.02
-.04
-.06
-.08
-1.0
ΔC1

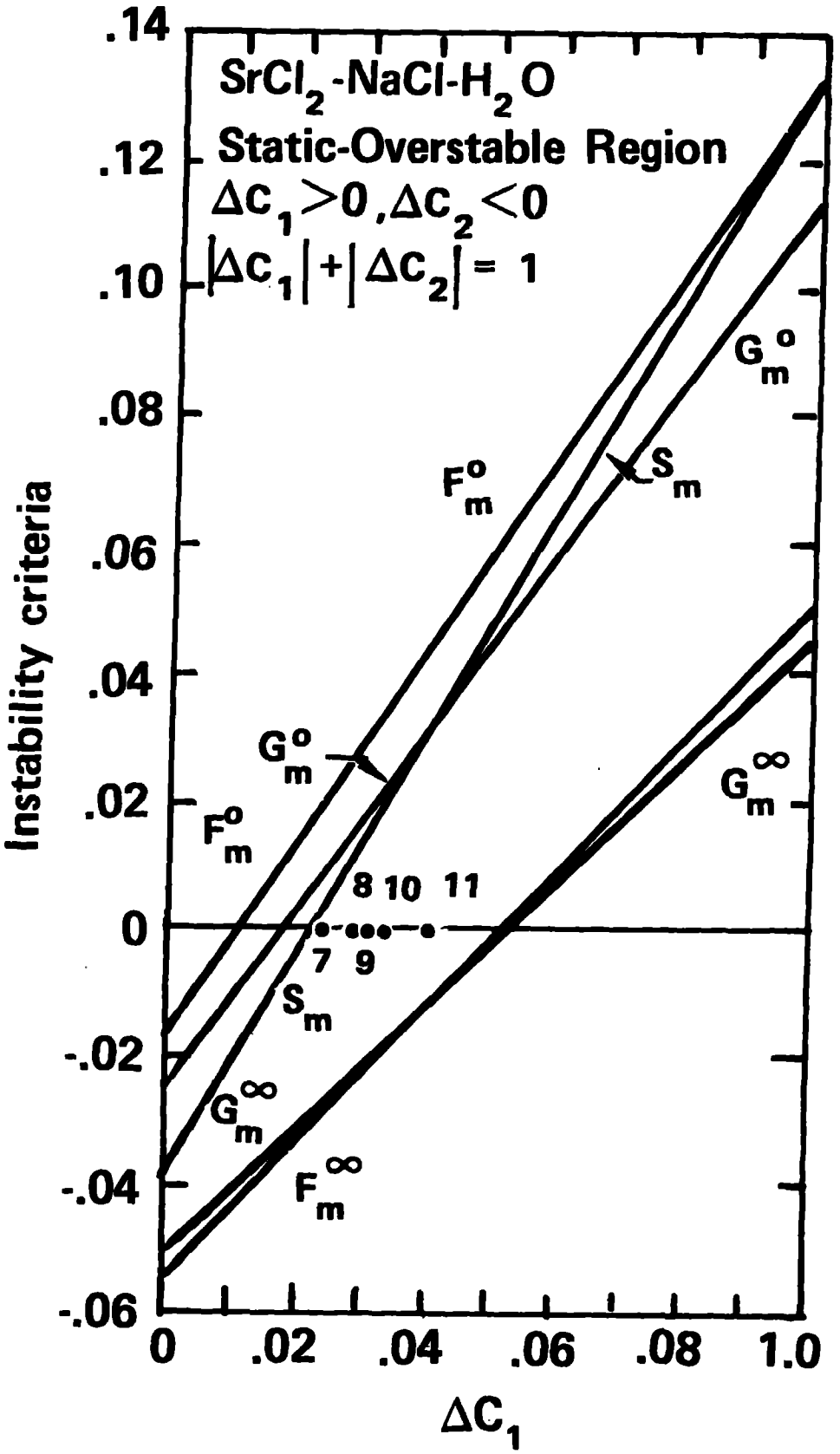
SrCl2-NaCl-H2O
Static-Overstable Region
ΔC1>0, ΔC2<0
|ΔC1|+|ΔC2| = 1
Instability criteria
ΔC1
.14
.12
.10
.08
.06
.04
.02
0
-.02
-.04
-.06
.02
.04
.06
.08
1.0
G°m
F°m
Sm
G°m
F°m
8 10 11
7 9
Sm
G∞m
F∞m
G∞m

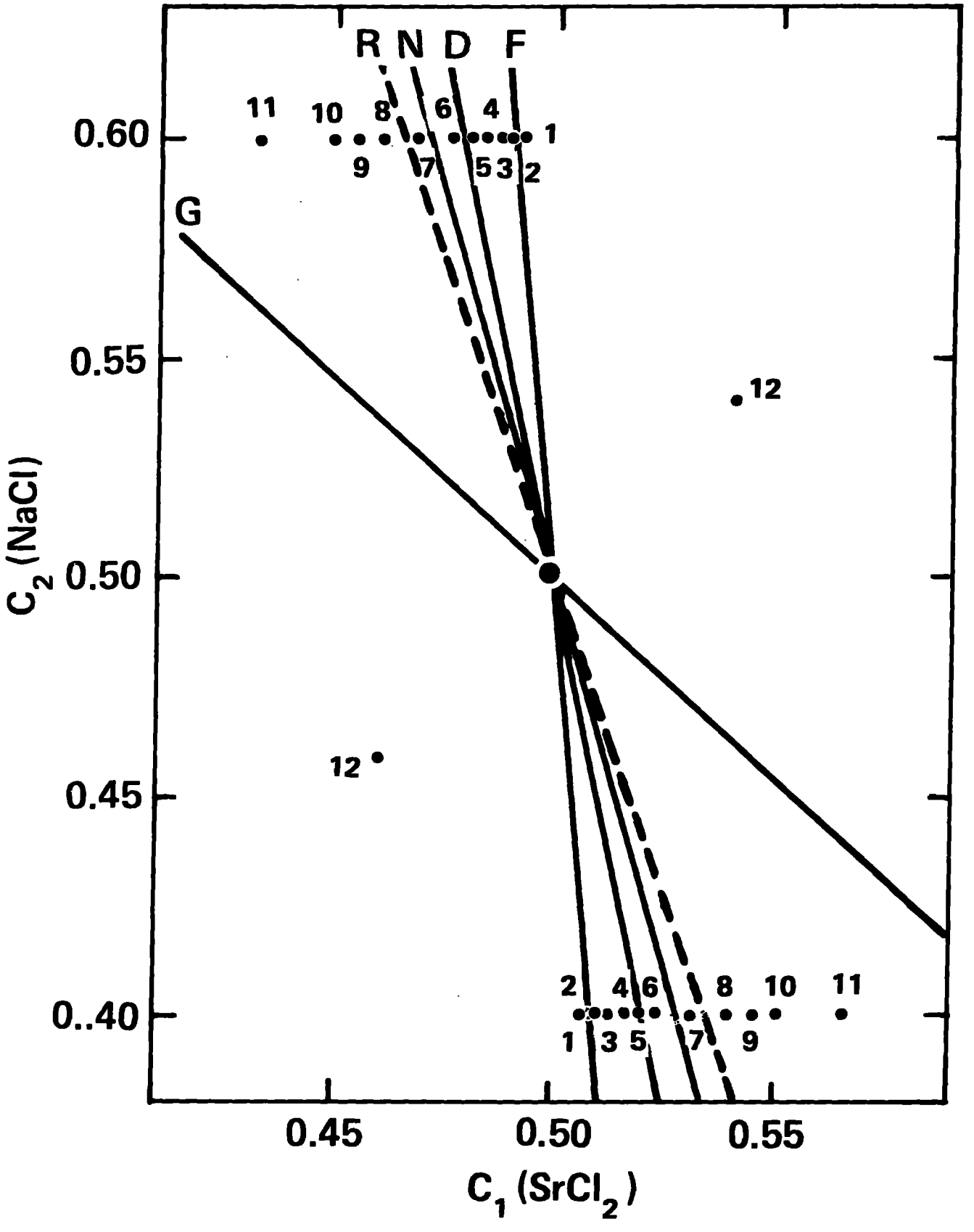
R N D F
G
11 10 8 6 4 1
9 7 5 3 2
12
12
2 4 6 8 10 11
1 3 5 7 9
0.60
0.55
0.50
0.45
0..40
0.45
0.50
0.55
C_2 (NaCl)
C_1 ($SrCl_2$)

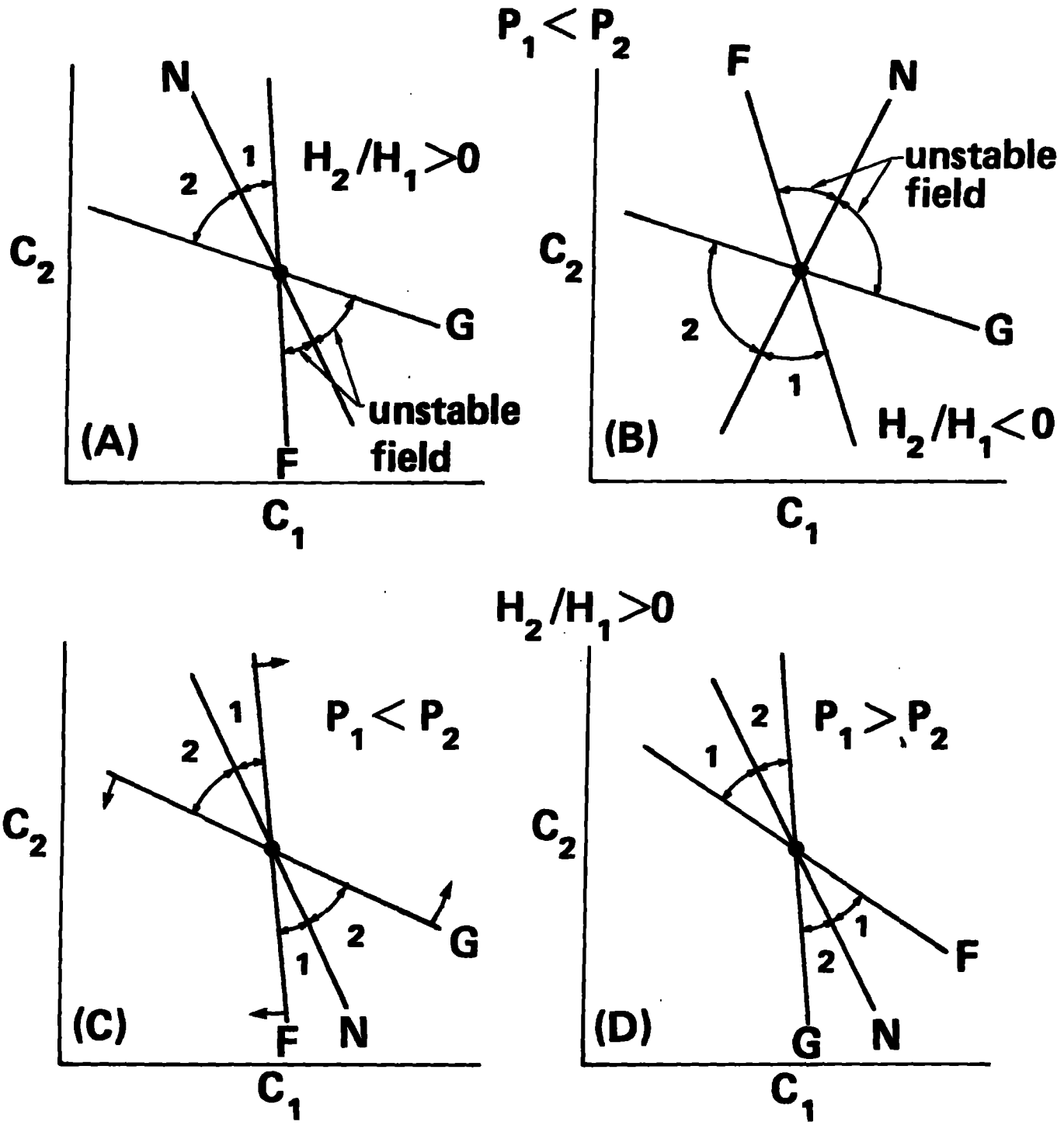
$P_1 < P_2$
N
1
2
$H_2/H_1 > 0$
C_2
G
unstable field
(A)
F
C_1
F
N
unstable field
C_2
G
2
1
(B)
$H_2/H_1 < 0$
C_1
$H_2/H_1 > 0$
1
2
$P_1 < P_2$
C_2
2
1
G
(C)
F
N
C_1
2
$P_1 > P_2$
1
C_2
1
2
F
(D)
G
N
C_1

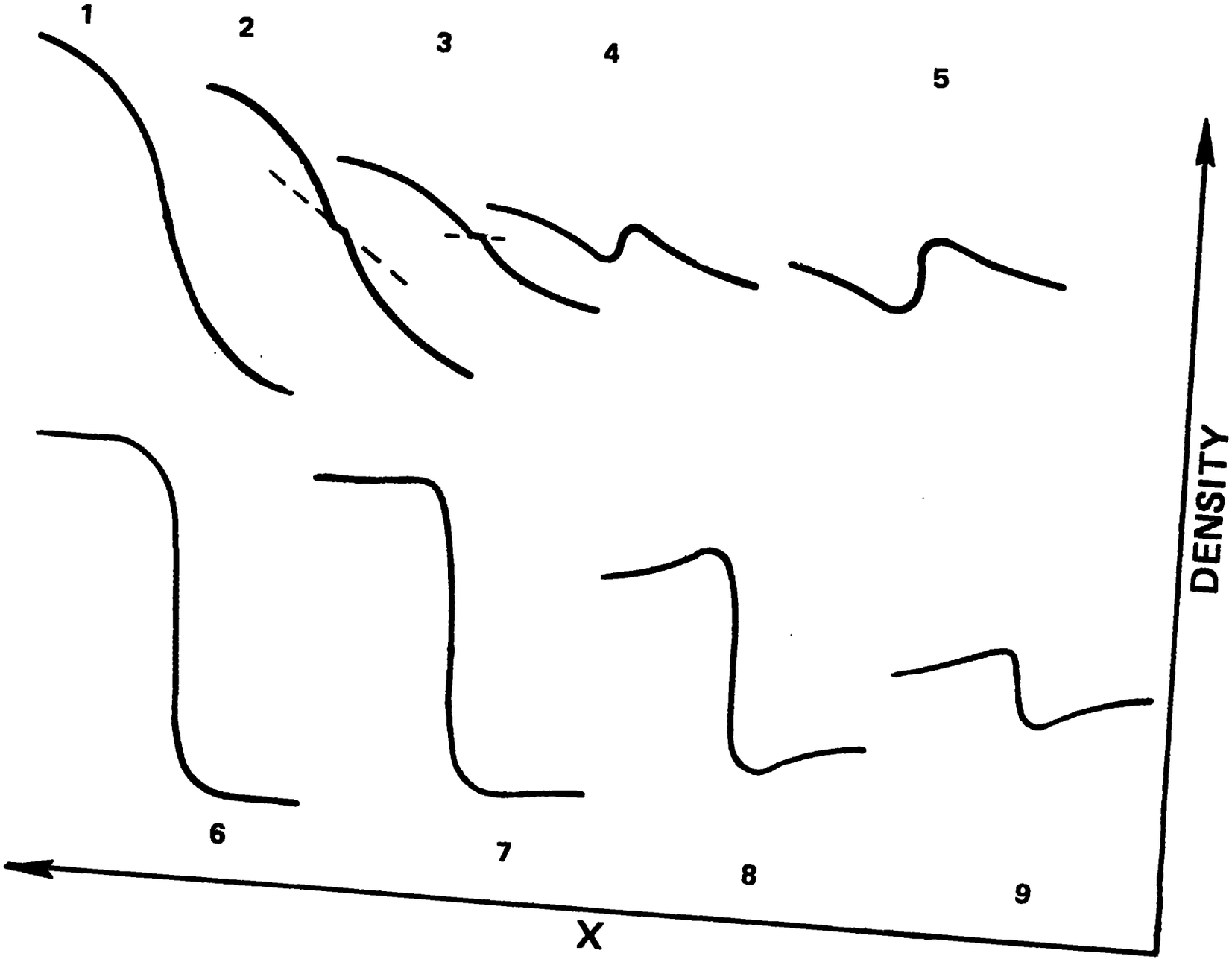
1
2
3
4
5
6
7
8
9
DENSITY
X

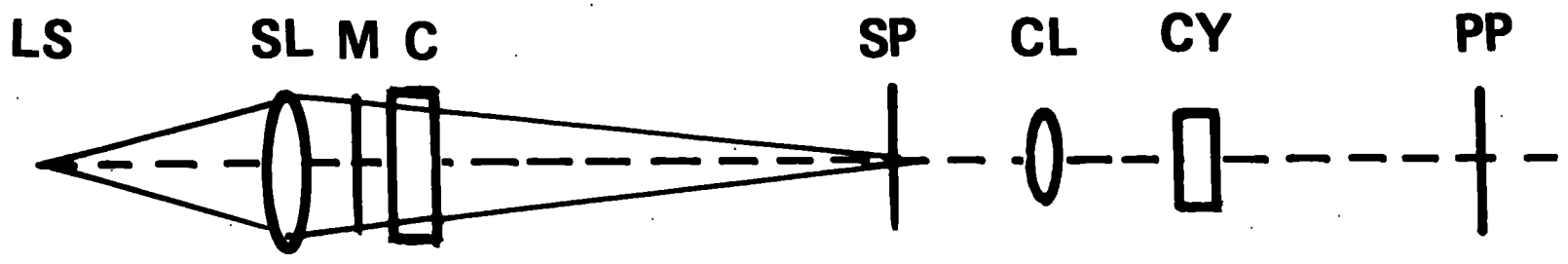

Convergent light Philpot-Svensson optics

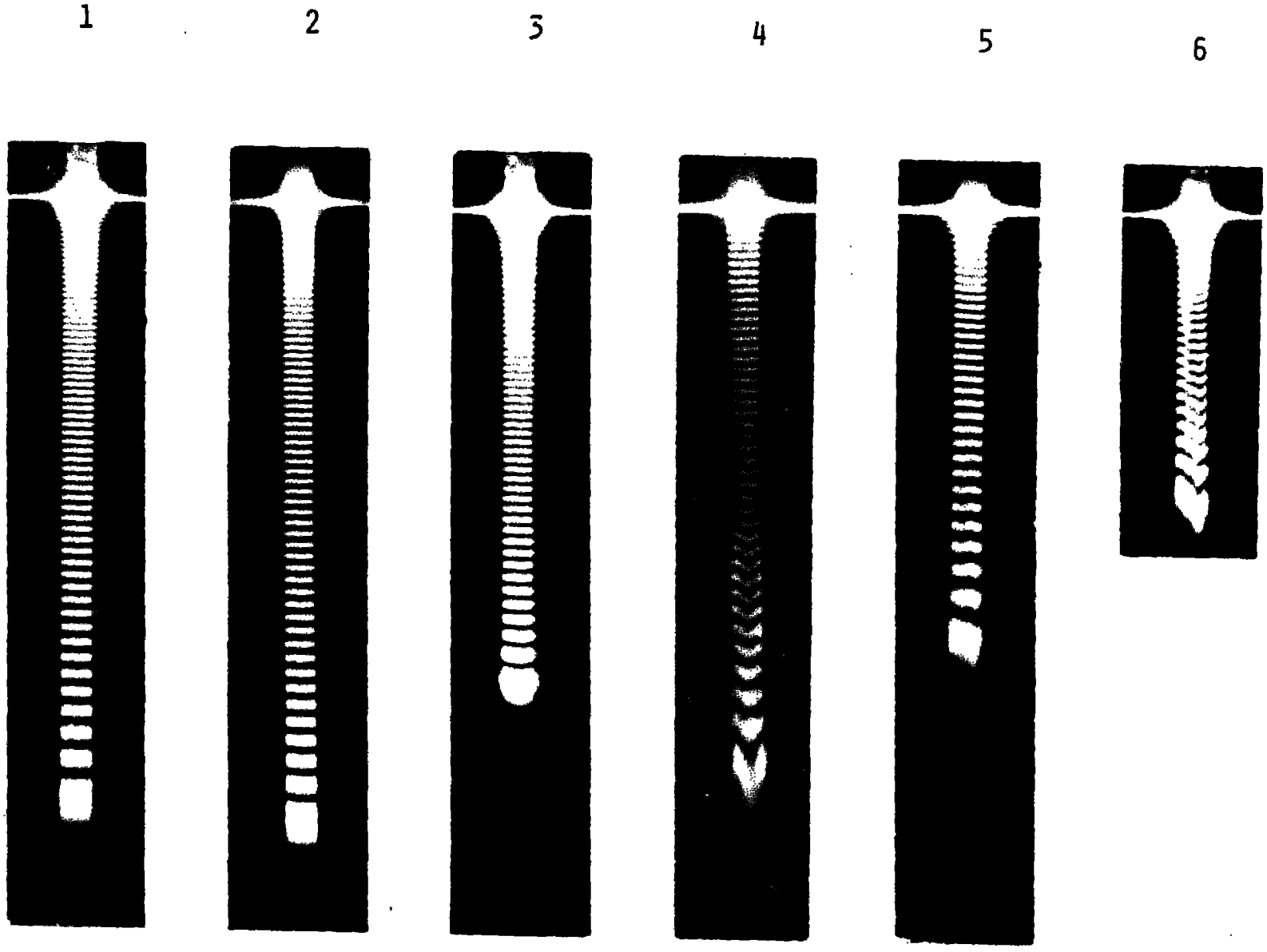
1
2
3
4
5
6

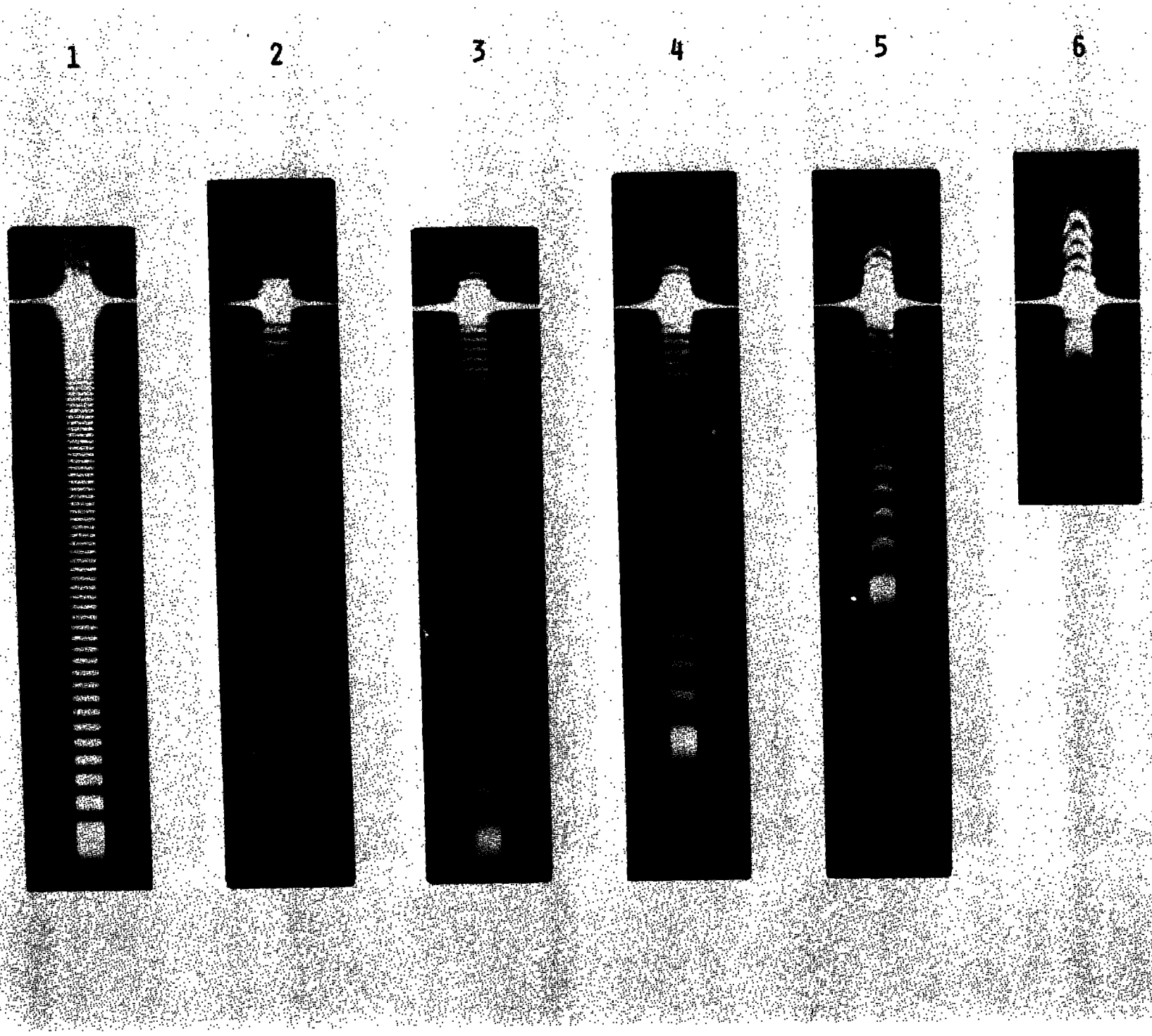
1
2
3
4
5
6

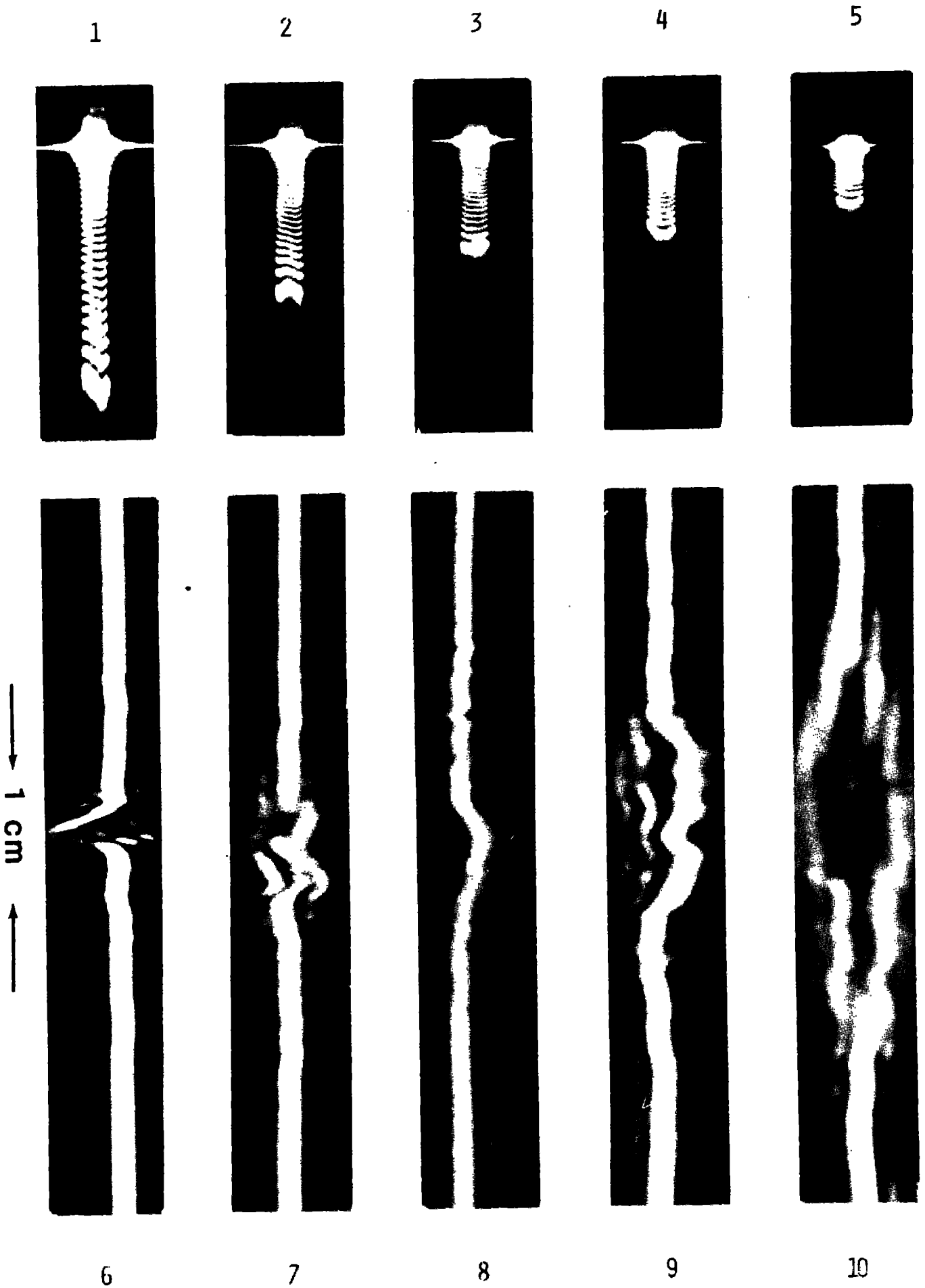
1
2
3
4
5
1 cm
6
7
8
9
10

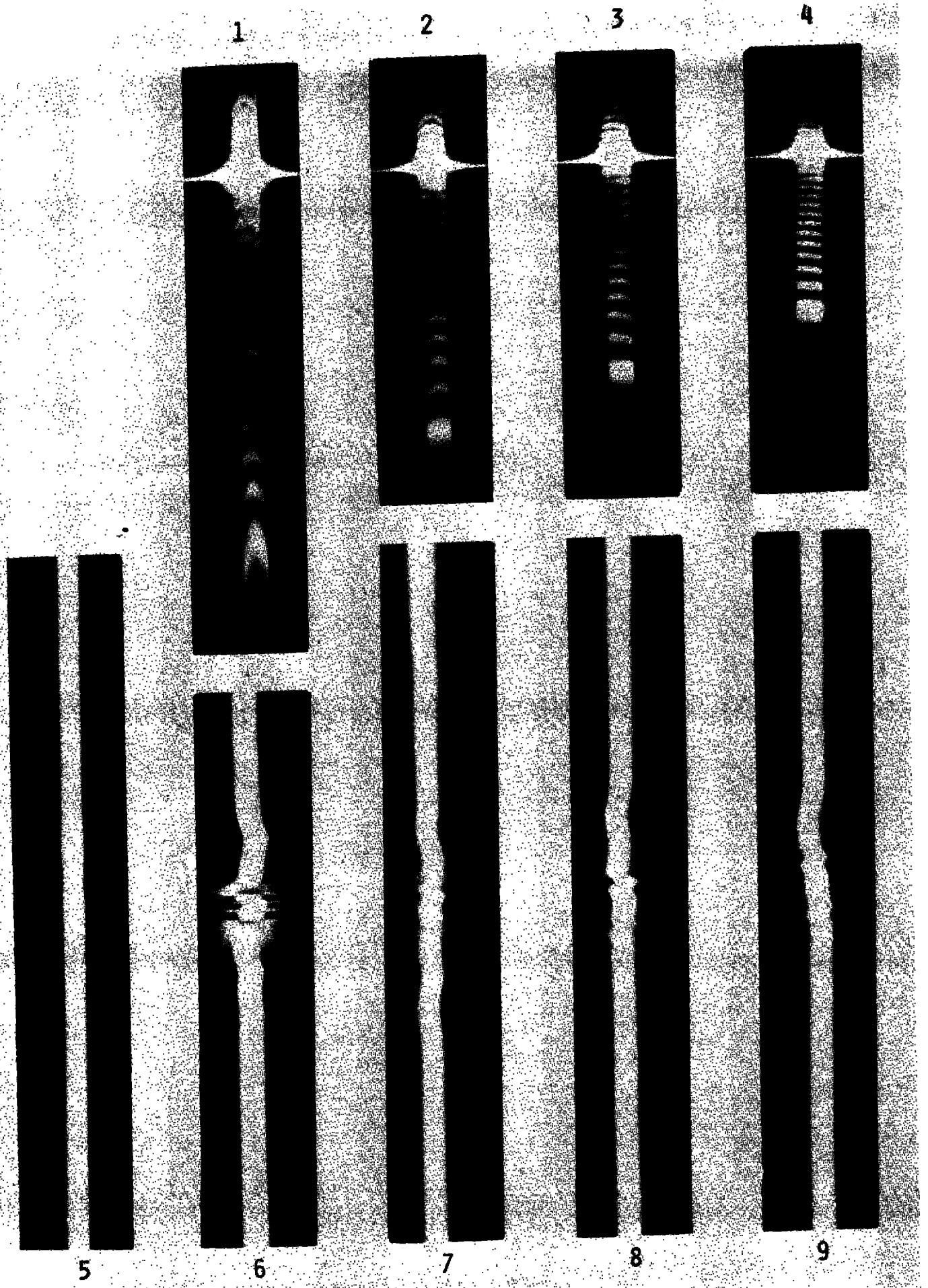
1
2
3
4
1 cm
5
6
7
8
9

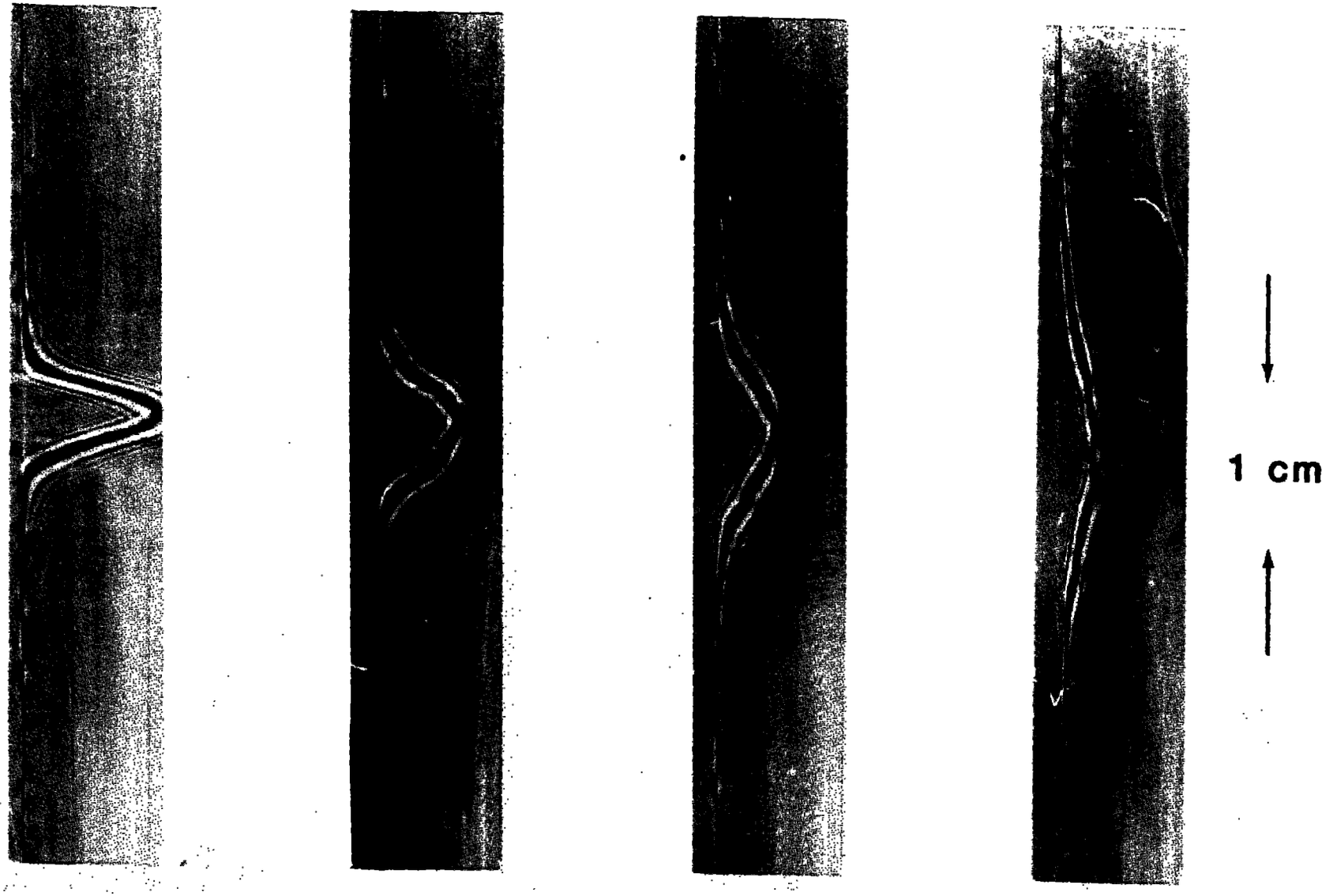

1 2 3 4

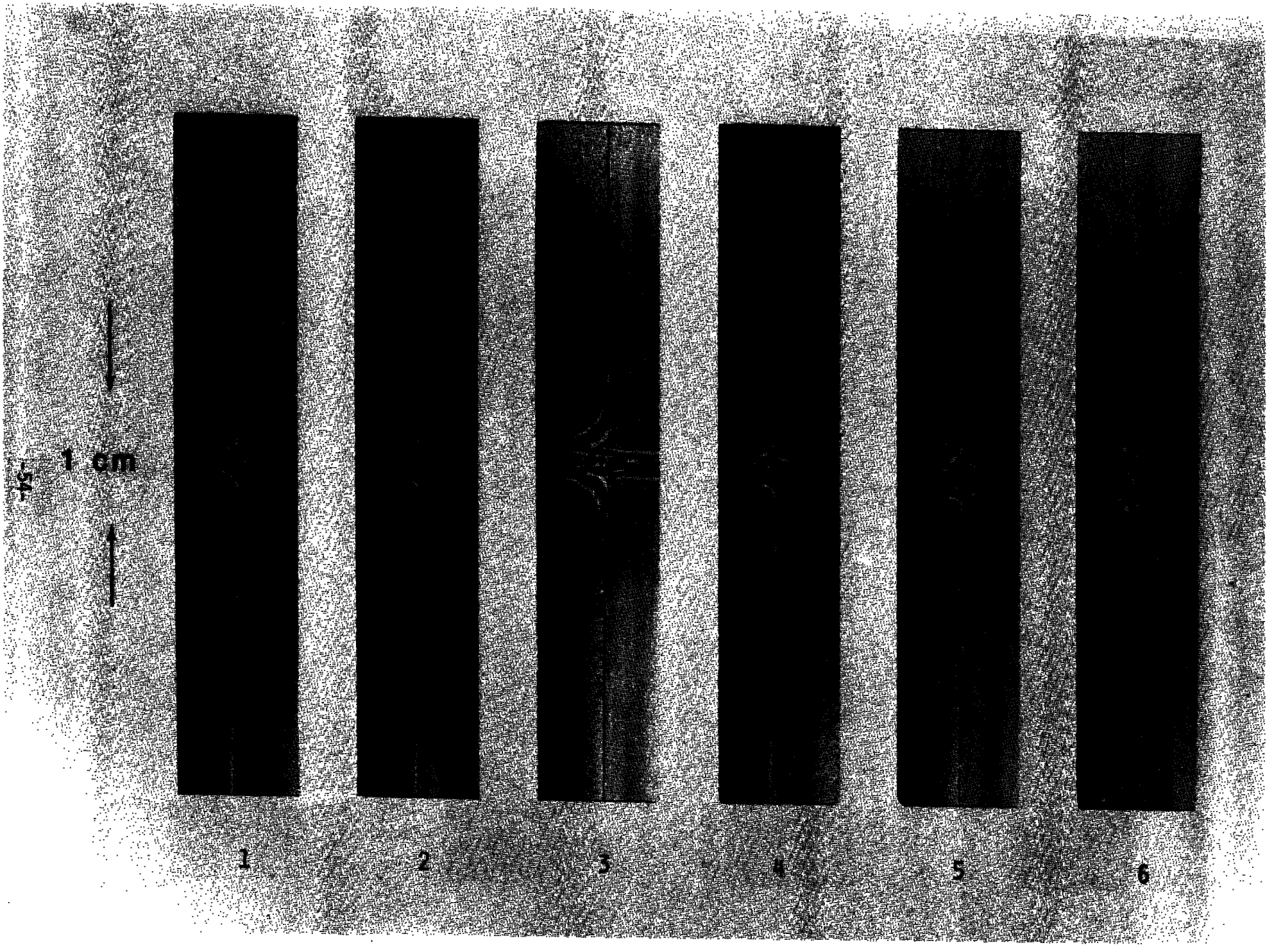
1 cm
1
2
3
4
5
6